1 μmol/L EDTA (pH 7.6)] supplemented with protease inhibitor cocktail Complete Mini (Roche Diagnostics). After centrifugation of the homogenates (3000*g* for 10 minutes), the supernatants or serum samples were used for measurement. To activate latent TGF-β_1 to an immunoreactive form, the samples were treated with acid according to the manufacturer's instructions (R&D Systems Inc). IL-10 or IL-6 concentrations in the sera and TGF-β_1, IL-6, HO-1, or TNF-α in the lung extracts were measured using enzyme-linked immunosorbent assay (ELISA) kits (Amersham Pharmacia Biotech; R&D Systems). The minimum detectable dose was 3, 3, 16, and 5 pg/mL or 0.78 ng/mL for IL-10, TGF-β_1, IL-6, and TNF-α, or HO-1, respectively. Inter- and intraassay precision of these kits was <10%. The total protein concentrations in the lung extracts were estimated using a BCA Protein Assay kit (PIERCE). The levels of TGF-β_1, IL-6, HO-1, or TNF-α in the lung were expressed as pg per mg protein.

Cell Culture and Proliferation Assay

Human PASMCs were obtained from Clonetics Corp and grown in SmGM-2 medium (Clonetics Corp). PASMCs with a passage between 4 and 6 were used in the experiments. Cells (1×10^3 per well) were incubated in 96-well plates with serum-free Dulbecco's modified Eagle's medium and nutrient mixture F12 (DMEM-F12, Invitrogen) in an atmosphere of 5% CO_2 in the air at 37°C. A tetrazolium-based colorimetric proliferation assay (XTT assay; Cell Proliferation Kit II, Roche Diagnostics) was performed 2 days after adding tin protoporphyrin IX (SnPP; Frontier Scientific), human recombinant TGF-β_1, IL-6, or IL-10 (PeproTech Inc). The optical density between 450 and 650 nm were measured to estimate the number of viable cells.

Statistical Analysis

Data from multiple experiments are expressed as mean±SEM. Statistical analysis and correlations were performed using StatView (Abacus Concepts, Inc). Survival curves were analyzed using the Kaplan–Meier method and compared by log-rank tests. Differences in other parameters were evaluated by analysis of variance combined with Fisher test. The correlation test was used to measure the association between 2 variables. A value of $P<0.05$ was considered statistically significant.

Results

AAV Vector-Mediated IL-10 Expression Improves Survival of MCT-PAH Rats

Eight weeks after AAV-IL-10 injection, serum IL-10 concentrations were elevated in a vector dose-dependent manner (Figure 1A). We determined that injection with AAV-IL-10 (6×10^{10} g.c. per rat) significantly increased serum IL-10 levels as compared with untreated controls (184.1±47.6 versus 18.8±1.3 pg/mL, $P<0.05$, n=3 each). In contrast, injection with MCT (Figure 1A) or AAV-eGFP alone (data not shown) caused no significant change in serum IL-10 levels. Therefore, we used this dosage for all vectors in subsequent experiments. For survival analysis, the rats were injected with a lethal dose of MCT, after 4 weeks of vector injection. The survival in IL-10–transduced rats was significantly improved as compared with the eGFP-transduced rats 8 weeks after MCT injection (75% versus 0%, $P<0.01$, n=8 each; Figure 1B).

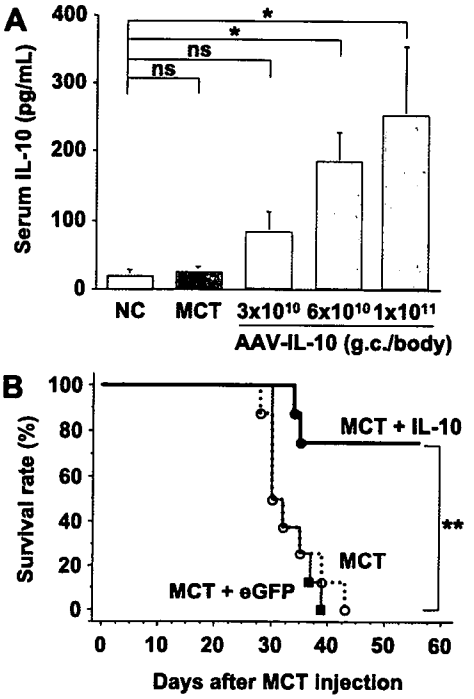

Figure 1. Adeno-associated virus (AAV) vector-mediated systemic interleukin (IL)-10 expression improves survival of monocrotaline (MCT)-induced pulmonary arterial hypertension (PAH) rats. A, In vivo IL-10 expression induced by AAV-IL-10. Serum IL-10 concentrations (pg/mL) were determined using ELISA 8 weeks after a single intramuscular injection of AAV-IL-10 into the anterior tibial muscles of 3-week-old Wistar rats. Genome copies (g.c.) per rat were as indicated. Data represent mean±SEM (n=3 animals per group, *$P<0.05$). ns indicates not statistically significant; NC, untreated controls. B, The Kaplan-Meier survival curve in MCT-PAH rats. The Wistar rats were treated with a lethal dose of MCT 4 weeks after the single intramuscular injection of HN buffer (MCT group), AAV-eGFP (MCT+eGFP group), or AAV-IL-10 (MCT+IL-10 group). n=8 animals per group, **$P<0.01$ versus MCT or MCT+eGFP groups.

Effects of IL-10 on PAH and RVH

Four weeks after MCT injection, the mPAP levels were significantly higher than those of the untreated controls (30.1±4.0 versus 20.0±2.1 mm Hg, $P<0.01$, n=5 each; Figure 2A). Treatment with AAV-IL-10 but not AAV-eGFP significantly inhibited the elevation of mPAP (22.8±1.5 versus 29.7±2.8 mm Hg, $P<0.01$, n=5 each; Figure 2A). Moreover, serum IL-10 concentrations correlated negatively with mPAP in MCT-treated rats ($r=-0.75$, $P<0.01$, n=15; Figure 2B). In contrast, this IL-10 expression caused no significant change in HR (data not shown) and mAoP (76.7±2.1 versus 74.6±6.8 mm Hg, MCT+IL-10 versus MCT+eGFP group, n=5 each). IL-10 expression also has a beneficial effect on RVH. Four-week MCT treatment significantly increased the RV/(LV+S) values as compared with the untreated controls ($P<0.01$, n=5 each; Figure 2C). Treatment with AAV-IL-10 but not AAV-eGFP inhibited MCT-induced increase of RV/(LV+S) significantly ($P<0.05$, n=5 each; Figure 2C). Furthermore, serum IL-10 concentrations correlated negatively with RV/(LV+S) in MCT-treated rats ($r=-0.57$, $P<0.05$, n=15; Figure 2D). These results indicate that sustained IL-10 expression prevented the development of MCT-induced PAH and RVH.

Effects of IL-10 on Histological Changes of the PA

Medial hypertrophy is a hallmark of pathological vascular remodeling in PAH. Four weeks after MCT injection, the medial thickness of PAs was markedly increased in the MCT-treated rats compared with untreated controls ($P<0.01$,

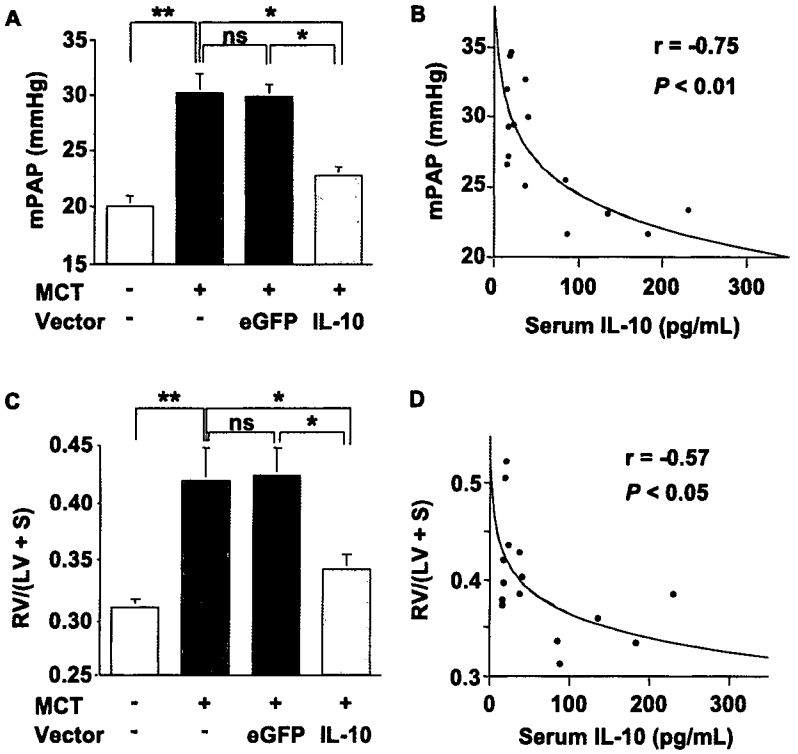

Figure 2. Effects of IL-10 on PAH and right ventricular hypertrophy (RVH). The 7-week-old Wistar rats were treated with monocrotaline (MCT) 4 weeks after vector injection. A, Statistical analysis of mean pulmonary arterial pressure (mPAP, mm Hg) determined by direct catheterization 4 weeks after MCT injection. Data represent the mean±SEM (n=5 animals per group; $^{*}P<0.05$, $^{**}P<0.01$). ns indicates not statistically significant. B, Correlation between serum IL-10 concentrations and mPAP levels in the MCT-treated rats (groups: MCT, MCT+eGFP, or MCT+IL-10; n=5 animals per group; $r=-0.75$, $P<0.01$). C, Quantitative RVH analysis. The weight ratio of the right ventricle to left ventricle plus septum [RV/(LV+S)] is presented as an index of RVH (n=5 animals per group; $^{*}P<0.05$, $^{**}P<0.01$). D, Correlation between serum IL-10 concentrations and RV/(LV+S) in the MCT-treated rats (groups: MCT, MCT+eGFP, and MCT+IL-10; n=5 animals per group; $r=-0.57$, $P<0.05$).

n=5 each; Figure 3B, 25 to 50 μm; Figure 3C, 51 to 100 μm in external diameter). Treatment with AAV-IL-10 but not AAV-eGFP significantly inhibited the increase in percent medial thickness ($P<0.01$, n=5 each). Inflammatory cell infiltration and vascular cell proliferation are also important indicators in the progression of PA remodeling. Immunohistochemical analysis shows that treatment with AAV-IL-10 significantly decreased the number of accumulated macrophages (ED1-positive cells; $P<0.01$, n=5 each; Figure 3D) and proliferating vascular cells (PCNA-positive cells; $P<0.01$, n=5 each; Figure 3E) in the PA of MCT-treated rats as compared with treatment with MCT alone or AAV-eGFP.

Effects of IL-10 on Cytokine Expression

We analyzed pulmonary tissue and serum cytokine levels relevant to the pathogenesis of PAH. Four weeks after MCT injection, the TGF-β_1 and IL-6 levels in the MCT-treated rats were significantly higher than those of the untreated controls ($P<0.01$, n=5 each; Figure 4A and 4C). Treatment with AAV-IL-10 but not AAV-eGFP significantly inhibited the MCT-induced elevation of TGF-β1 and IL-6 levels ($P<0.01$, n=5 each). Furthermore, these levels correlated positively with the percent medial thickness in the rats with or without MCT treatment ($r=0.84$, $P<0.01$; $r=0.87$, $P<0.01$, respectively; Figure 4B and 4D).

HO-1 has been reported to mediate the antiinflammatory effects of IL-10.[24] Treatment with AAV-IL-10 but not AAV-eGFP or MCT alone significantly increased the lung HO-1 levels as compared with untreated controls ($P<0.05$, n=5 each, Figure 4E). In addition, HO-1 levels correlated negatively with IL-6 levels in MCT-treated rats ($r=-0.85$, $P<0.01$; Figure 4F). In contrast, serum IL-6 levels positively correlated with lung IL-6 levels ($r=-0.69$, $P<0.01$; Figure 4G). Although the lung TNF-α levels significantly increased in MCT-treated rats compared with untreated controls, IL-10 expression caused no change in the lung TNF-α levels (Figure 4H).

Effects of IL-10 on PASMC Proliferation

To determine whether IL-10 directly inhibits PASMC proliferation, we performed an in vitro colorimetric XTT assay using cultured human PASMCs. Treatment of PASMCs with SnPP, which inactivates HO-1, and treatment with TGF-β_1 or IL-6 dose dependently promoted cell proliferation (n=4 each, $P<0.05$; Figure 5A through 5C). Treatment with IL-10 alone had no significant effect on PASMC proliferation (Figure 5D). On the other hand, pretreatment with IL-10 significantly inhibited PASMC proliferation induced by SnPP or TGF-β_1 (n=4 each, $P<0.05$; Figure 5E) but not that induced by IL-6.

Discussion

The present study demonstrates that IL-10, delivered by an intramuscular injection of an AAV1 vector, prevented the development of MCT-PAH in rats. Systemic IL-10 expression also improved survival in rats and prevented the development of RVH and medial hypertrophy of PA. IL-10 also reduced macrophage accumulation, vascular cell proliferation, and pulmonary tissue levels of TGF-β_1 and IL-6, all of which play pivotal roles in progression of PA remodeling. Further, IL-10 enhanced HO-1 levels in the lung. Thus, IL-10 exerts multiple preventive effects on inflammatory and proliferative PA remodeling (Figure 6).

Blockade of a single proinflammatory signaling pathway by IL-1 or monocyte chemoattractant protein-1 attenuates PA remodeling.[25,26] However, the prosurvival effects of antiinflammatory molecules on PAH animals have not been re-

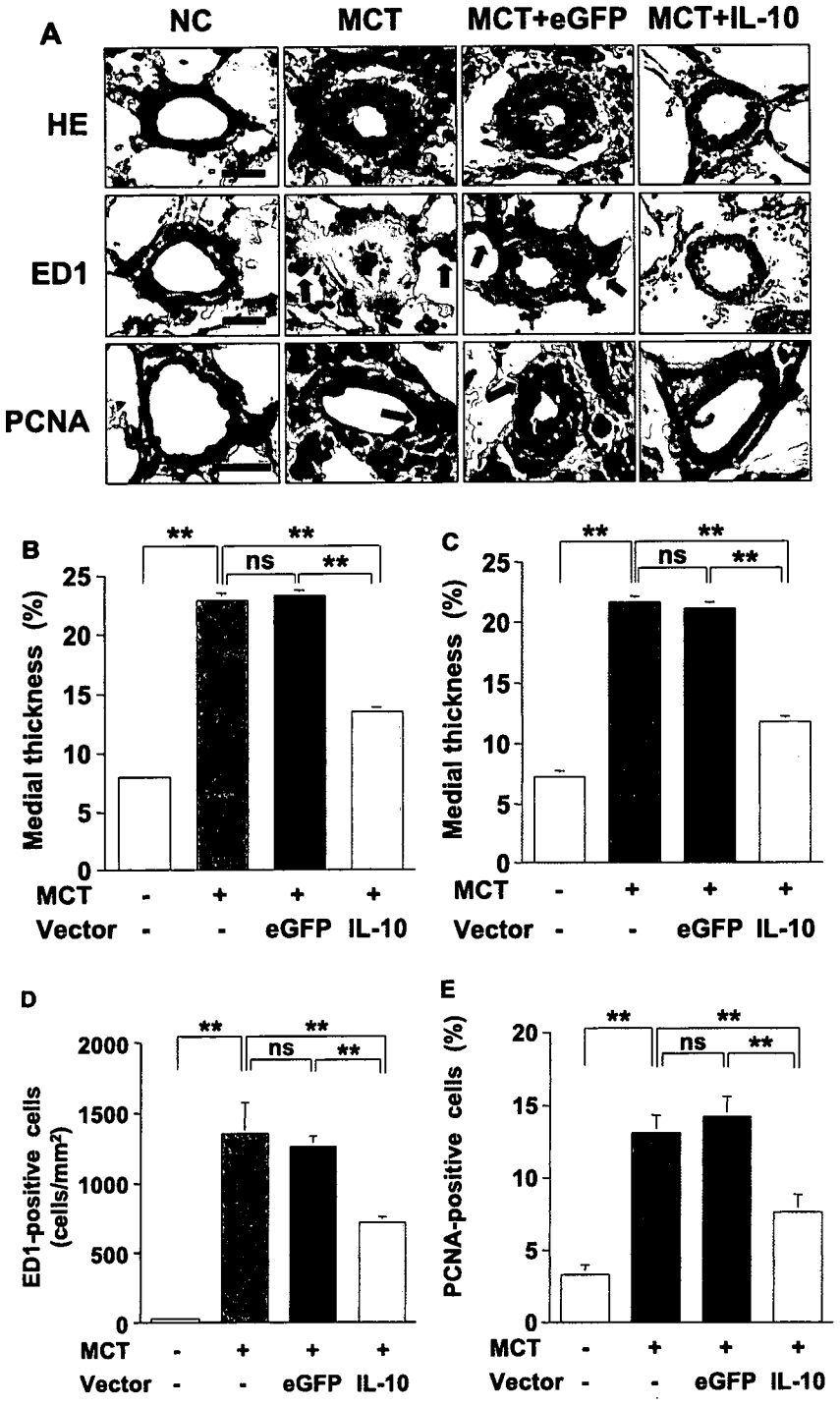

Figure 3. Antiinflammatory and antiproliferative effects of IL-10 on the remodeled pulmonary artery (PA). The 7-week-old Wistar rats were treated with MCT 4 weeks after vector injection. Representative cross-sectional views of the peripheral PAs stained with HE or immunohistochemistry (ED1 or PCNA) 4 weeks after MCT treatment (A; original magnification ×1000, Scale bar=20 μm). Blue arrows indicate ED-1–positive cells and red arrows, PCNA-positive cells. Quantification of percent medial thickness for vessels 25 to 50 μm (B) and 51 to 100 μm (C) in external diameter. Quantitative analysis of the number of perivascular macrophages (ED-1–positive cells, D) and proliferating vascular cells (PCNA-positive cells, E). Data represent mean±SEM (n=5 animals per group, $^{**}P<0.01$). ns indicates not statistically significant.

ported. Evidence of right heart failure is involved in the mortality of MCT-PAH rats. In this study, all rats treated with a lethal dose of MCT exhibited symptoms of right heart failure such as pleural effusion and body weight decrease. In the setting of severe PAH and right heart failure, cytokine networks may orchestrate disease progression. Thus, blockades of multiple inflammatory signals might be responsible for the prosurvival effect of IL-10.

IL-10 has gained significant attention because of its suppressive influence on inflammatory and proliferative vasculopathy. The IL-10 receptor is expressed on vascular smooth muscle cells (VSMCs). IL-10 inhibits inflammation and VSMC proliferation in arterial remodeling after balloon injury or transplant rejection.[12,13] Consistent with previous studies using MCT-PAH,[6,7] we demonstrate that increased levels of TGF-β_1 and IL-6 are related to PASMC proliferation and PA remodeling progression. Although treatment with IL-10 alone caused no significant effects on PASMC proliferation,[27] IL-10 significantly inhibited the lung TGF-β_1 expression and TGF-β_1-induced PASMC proliferation. TGF-β_1 enhances PASMC proliferation of idiopathic PAH patients but not that of normal subjects or secondary PAH patients.[28]

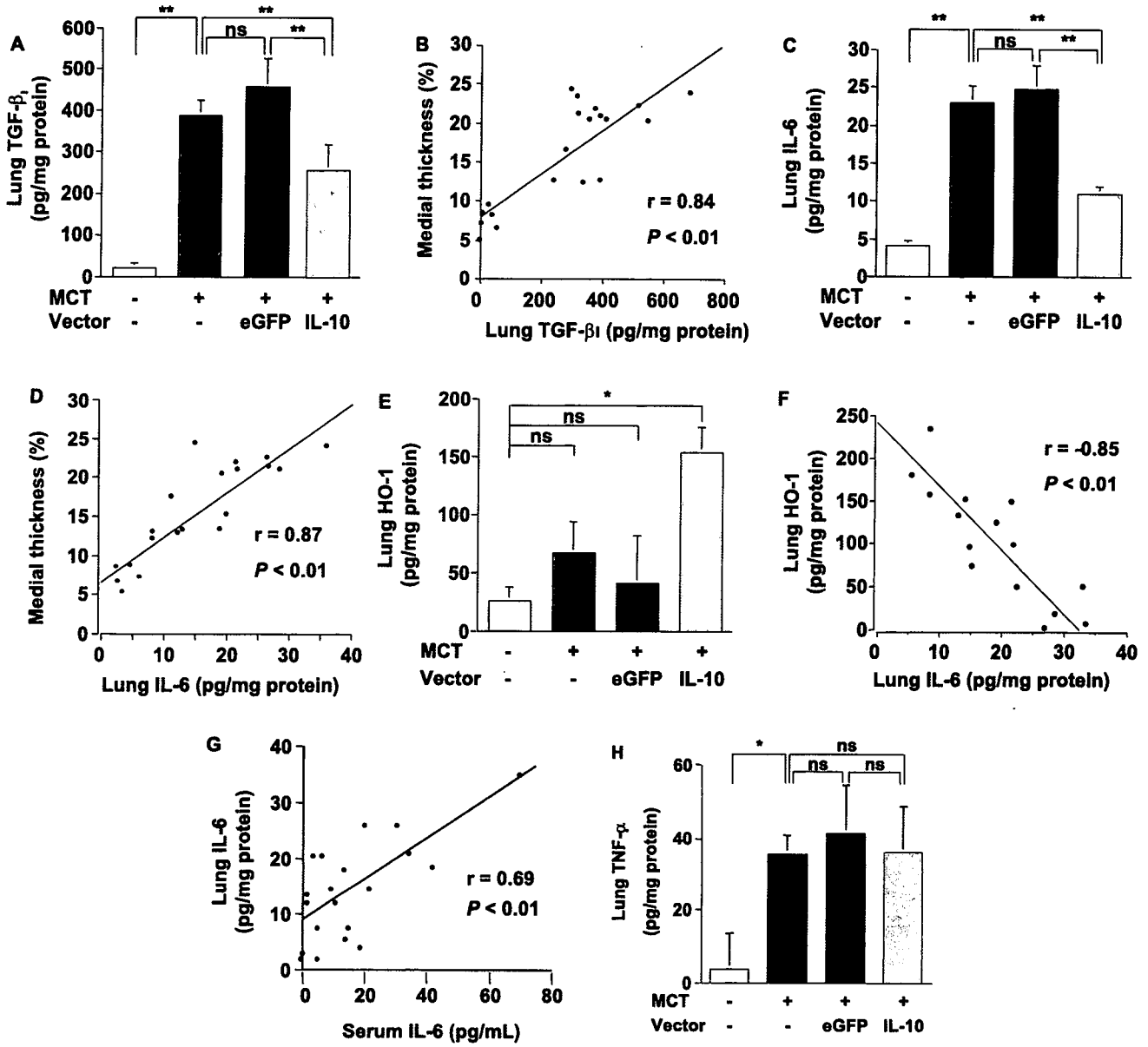

Figure 4. Effects of IL-10 on expression of transforming growth factor-β_1 (TGF-β_1), IL-6, heme oxygenase-1 (HO-1), and tumor necrosis factor-α (TNF-α) in the lung. The 7-week-old Wistar rats were treated with MCT 4 weeks after vector injection. Concentrations of active TGF-β_1 (A), IL-6 (C), HO-1 (E), and TNF-α (H) in the lung extracts were detected using ELISA 4 weeks after MCT treatment. Data represent mean±SEM (n=5 animals per group; *P<0.05, **P<0.01). ns indicates not statistically significant. Correlation between the percent medial thickness and lung levels of TGF-β_1 (B) or IL-6 (D) in rats (groups: NC, MCT, MCT+eGFP, or MCT+IL-10; n=5 animals per group; r=0.84, P<0.01 and r=0.87, P<0.01, respectively). Correlation between the HO-1 and IL-6 (F) levels in the rat lung (groups: MCT, MCT+eGFP, or MCT+IL-10; n=5 animals per group; r=−0.85, P<0.01). Correlation between the lung and serum IL-6 levels (G) in rats (groups: NC, MCT, MCT+eGFP, or MCT+IL-10; n=5 animals per group; r=0.69, P<0.01).

Additionally, TGF-β_1 is accumulated in the hypertrophic PA of both human PAH and MCT-PAH[29,30] and exacerbates PA remodeling.[31]

IL-6, a multifunctional proinflammatory cytokine, acts as a strong mitogen to promote VSMC proliferation.[11] Macrophage infiltration is a hallmark of PAH progression, and activated macrophages produce substantial amounts of IL-6 in MCT-PAH rats.[6,32] In this study, IL-10 treatment inhibited perivascular macrophage infiltration and the lung IL-6 expression in vivo but not IL-6-induced PASMC proliferation in vitro. These results suggest that IL-10 may attenuate IL-6 function indirectly through the decreased accumulation of perivascular macrophages and IL-6. Furthermore, the serum IL-6 levels significantly correlated with the lung IL-6 levels. Because serum IL-6 level reflects the disease activity of idiopathic PAH, it can be a useful biomarker of antiinflammation therapy of PAH. On the other hand, IL-10 did not affect the MCT-induced TNF-α expression in the lung. However, previous studies demonstrated that IL-10 prevents TNF-α–induced VSMC proliferation in vitro.[27] These observations suggest that IL-10 might modulate the downstream signal of TNF-α but not its expression in the setting of MCT-PAH. Overall, IL-10 affects the dynamics of cytokine networks involved in PA remodeling, and its site of action may differ according to the cytokine signal.

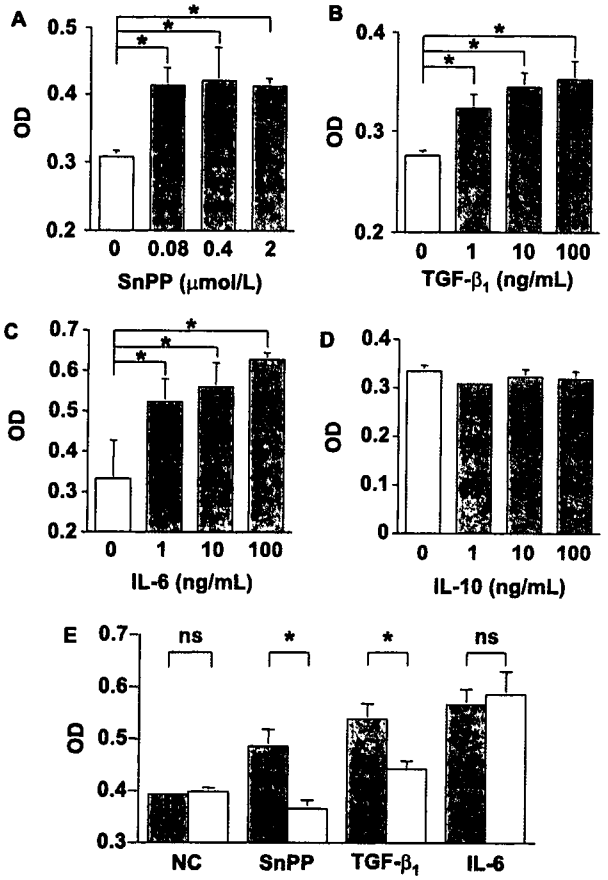

Figure 5. Antiproliferative effects of IL-10 on pulmonary arterial smooth muscle cells (PASMCs). The number of viable human PASMCs cultured in serum-free DMEM-F12 was estimated using a colorimetric assay (XTT assay). The optical density (OD) between 450 nm and 650 nm indicates the extent of cell proliferation. Addition of tin protoporphyrin IX (SnPP, A), TGF-β_1 (B), or IL-6 (C) dose-dependently promotes PASMC proliferation. Although IL-10 alone has no significant effect (D), pretreatment with IL-10 (10 ng/mL) inhibits PASMC proliferation induced by SnPP (2 μmol/L) or TGF-β_1 (20 ng/mL, E) but not that induced by IL-6 (20 ng/mL). Closed columns, cells not treated with IL-10; open columns, IL-10–treated cells. The results are representative of 3 independent experiments. Data represent mean±SEM (n=4 each, *P<0.05). ns indicates not statistically significant.

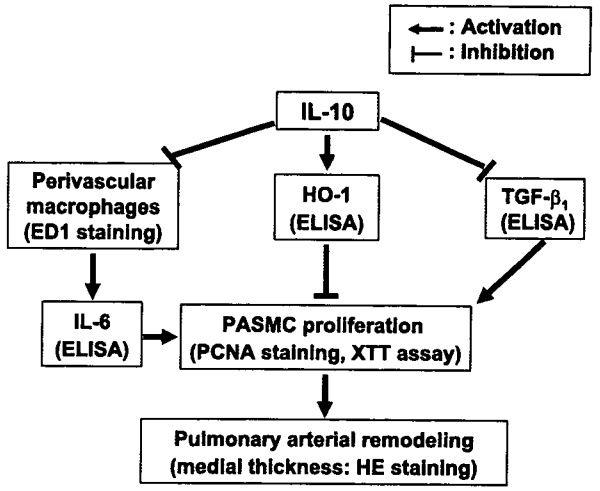

Figure 6. Proposed explanation for IL-10–mediated prevention of PAH and vascular remodeling. Monocrotaline treatment causes PAH in rats by inducing inflammation and proliferation of the PA. IL-10 prevents the development of PAH and PA remodeling by inhibiting vascular inflammation and proliferation. The effects of IL-10 are related to the decreased accumulation of perivascular macrophages and the reduced levels of active TGF-β_1 and IL-6. IL-10 induces HO-1 expression, which can negatively regulate inflammation and proliferation in the PA. IL-10 inhibits abnormal proliferation of PASMCs, thereby preventing PAH development.

CO induced by HO-1 blocks PASMC proliferation not only directly by inhibiting the expression of a cell cycle–specific transcription factor but also indirectly by attenuating mitogen signaling.[16] Interestingly, the transgenic mice that constitutively express HO-1 are protected from the development of hypoxia-induced PAH and excessive expression of a mitogen IL-6.[33] In this study, AAV-IL-10 administration increased the HO-1 level that negatively correlated with the IL-6 level in the lung of MCT-PAH rats. These observations suggest a dynamic relationship between IL-6 and HO-1 in PA remodeling progression. Chen et al[12] reported that AAV-IL-10 injection enhanced the activity and protein levels of HO-1, but SnPP treatment that inactivates HO-1 reversed the vasculoprotective effects of IL-10 in vivo. Here, we show that pretreatment with recombinant IL-10 suppressed the excessive PASMC proliferation induced by HO-1 inactivation with SnPP. Thus, IL-10 may sustain CO levels by maintaining HO-1 from inactivating, leading to the prevention of PA remodeling.

Finally, we will discuss the clinical implication and limitations of this study. Consistent with previous studies, maximum gene expression was noted 6 to 8 weeks after the intramuscular injection of AAV vectors. In this study, AAV-IL-10 was injected 4 weeks before MCT administration for the transgene expression to reach plateau levels when MCT-PAH was fully developed (3 to 4 weeks after the injection). Thus, our results are completely based on a prevention protocol, which may be rare in a clinical setting. Intramuscular AAV-IL-10 injection is an attractive candidate for antiinflammation therapy of PAH because inflammatory cytokine expression is associated with the clinical course of the disease. In addition, this strategy exhibited no life-threatening complications such as shock and sepsis which may occur in intravenous prostacyclin infusion therapy. However, therapeutic effects of IL-10 in established PAH has not been determined. Therefore, it should be further examined in studies using a treatment protocol. MCT-PAH is a widely-used and suitable model for exploring inflammatory mechanisms in PAH progression. However, how IL-10 affects other pathogenesis in PAH remains unknown. In the future, IL-10 function needs to be examined in other PAH models such as hypoxia-induced PAH.

In conclusion, AAV vector-mediated sustained IL-10 expression prevented the development of MCT-PAH in rats. The antiremodeling effects of IL-10 are related to the reduction of macrophage infiltration and pathological cytokine expression as well as increased HO-1 levels in the lung. Although the therapeutic role of IL-10 should be further investigated, our results provide new insights into molecular mechanisms underlying the development of human PAH.

Acknowledgments

We thank Miyoko Mitsu for her encouragement and technical support.

Sources of Funding

This work was supported by grants from (1) the Ministry of Health, Labor and Welfare of Japan; (2) Grants-in-Aid for Scientific Research; (3) grant for 21 Century COE Program; (4) "High-Tech Research Center" Project for Private Universities, matching fund subsidy, from the Ministry of Education, Culture, Sports, Science and Technology of Japan; and (5) The Research Award to Jichi Medical School Graduate Student.

Disclosures

None.

References

1. Humbert M, Sitbon O, Simonneau G. Treatment of pulmonary arterial hypertension. *N Engl J Med.* 2004;351:1425–1436.
2. Stenmark KR, Fagan KA, Frid MG. Hypoxia-induced pulmonary vascular remodeling: cellular and molecular mechanisms. *Circ Res.* 2006; 99:675–691.
3. Tuder RM, Groves B, Badesch DB, Voelkel NF. Exuberant endothelial cell growth and elements of inflammation are present in plexiform lesions of pulmonary hypertension. *Am J Pathol.* 1994;144:275–285.
4. Humbert M, Monti G, Brenot F, Sitbon O, Portier A, Grangeot-Keros L, Duroux P, Galanaud P, Simonneau G, Emilie D. Increased interleukin-1 and interleukin-6 serum concentrations in severe primary pulmonary hypertension. *Am J Respir Crit Care Med.* 1995;151:1628–1631.
5. Miyata M, Sakuma F, Yoshimura A, Ishikawa H, Nishimaki T, Kasukawa R. Pulmonary hypertension in rats. 2. Role of interleukin-6. *Int Arch Allergy Immunol.* 1995;108:287–291.
6. Miyata M, Sakuma F, Yoshimura A, Ishikawa H, Nishimaki T, Kasukawa R. Pulmonary hypertension in rats. 1. Role of bromodeoxyuridine-positive mononuclear cells and alveolar macrophages. *Int Arch Allergy Immunol.* 1995;108:281–286.
7. Arcot SS, Lipke DW, Gillespie MN, Olson JW. Alterations of growth factor transcripts in rat lungs during development of monocrotaline-induced pulmonary hypertension. *Biochem Pharmacol.* 1993;46: 1086–1091.
8. Karmochkine M, Wechsler B, Godeau P, Brenot F, Jagot JL, Simonneau G. Improvement of severe pulmonary hypertension in a patient with SLE. *Ann Rheum Dis.* 1996;55:561–562.
9. Bellotto F, Chiavacci P, Laveder F, Angelini A, Thiene G, Marcolongo R. Effective immunosuppressive therapy in a patient with primary pulmonary hypertension. *Thorax.* 1999;54:372–374.
10. Ito T, Ozawa K, Shimada K. Current drug targets and future therapy of pulmonary arterial hypertension. *Curr Med Chem.* 2007;14:719–733.
11. Ito T, Ikeda U. Inflammatory cytokines and cardiovascular disease. *Curr Drug Targets Inflamm Allergy.* 2003;2:257–265.
12. Chen S, Kapturczak MH, Wasserfall C, Glushakova OY, Campbell-Thompson M, Deshane JS, Joseph R, Cruz PE, Hauswirth WW, Madsen KM, Croker BP, Berns KI, Atkinson MA, Flotte TR, Tisher CC, Agarwal A. Interleukin 10 attenuates neointimal proliferation and inflammation in aortic allografts by a heme oxygenase-dependent pathway. *Proc Natl Acad Sci U S A.* 2005;102:7251–7256.
13. Mazighi M, Pelle A, Gonzalez W, Mtairag el M, Philippe M, Henin D, Michel JB, Feldman LJ. IL-10 inhibits vascular smooth muscle cell activation *in vitro* and *in vivo*. *Am J Physiol Heart Circ Physiol.* 2004; 287:H866–H871.
14. Yoshioka T, Okada T, Maeda Y, Ikeda U, Shimpo M, Nomoto T, Takeuchi K, Nonaka-Sarukawa M, Ito T, Takahashi M, Matsushita T, Mizukami H, Hanazono Y, Kume A, Ookawara S, Kawano M, Ishibashi S, Shimada K, Ozawa K. Adeno-associated virus vector-mediated interleukin-10 gene transfer inhibits atherosclerosis in apolipoprotein E-deficient mice. *Gene Ther.* 2004;11:1772–1779.
15. Li MC, He SH. IL-10 and its related cytokines for treatment of inflammatory bowel disease. *World J Gastroenterol.* 2004;10:620–625.
16. Morita T, Mitsialis SA, Koike H, Liu Y, Kourembanas S. Carbon monoxide controls the proliferation of hypoxic vascular smooth muscle cells. *J Biol Chem.* 1997;272:32804–32809.
17. Christou H, Morita T, Hsieh CM, Koike H, Arkonac B, Perrella MA, Kourembanas S. Prevention of hypoxia-induced pulmonary hypertension by enhancement of endogenous heme oxygenase-1 in the rat. *Circ Res.* 2000;86:1224–1229.
18. Yun S, Junbao D, Limin G, Chaomei Z, Xiuying T, Chaoshu T. The regulating effect of heme oxygenase/carbon monoxide on hypoxic pulmonary vascular structural remodeling. *Biochem Biophys Res Commun.* 2003;306:523–529.
19. Matsushita T, Elliger S, Elliger C, Podsakoff G, Villarreal L, Kurtzman GJ, Iwaki Y, Colosi P. Adeno-associated virus vectors can be efficiently produced without helper virus. *Gene Ther.* 1998;5:938–945.
20. Okada T, Nomoto T, Yoshioka T, Nonaka-Sarukawa M, Ito T, Ogura T, Iwata-Okada M, Uchibori R, Shimazaki K, Mizukami H, Kume A, Ozawa K. Large-scale production of recombinant viruses by use of a large culture vessel with active gassing. *Hum Gene Ther.* 2005;16:1212–1218.
21. Okada T, Nomoto T, Shimazaki K, Lijun W, Lu Y, Matsushita T, Mizukami H, Urabe M, Hanazono Y, Kume A, Muramatsu S, Nakano I, Ozawa K. Adeno-associated virus vectors for gene transfer to the brain. *Methods.* 2002;28:237–247.
22. Kay JM, Keane PM, Suyama KL, Gauthier D. Angiotensin converting enzyme activity and evolution of pulmonary vascular disease in rats with monocrotaline pulmonary hypertension. *Thorax.* 1982;37:88–96.
23. Yoshioka T, Ageyama N, Shibata H, Yasu T, Misawa Y, Takeuchi K, Matsui K, Yamamoto K, Terao K, Shimada K, Ikeda U, Ozawa K, Hanazono Y. Repair of infarcted myocardium mediated by transplanted bone marrow-derived $CD34^+$ stem cells in a nonhuman primate model. *Stem Cells.* 2005;23:355–364.
24. Lee TS, Chau LY. Heme oxygenase-1 mediates the anti-inflammatory effect of interleukin-10 in mice. *Nat Med.* 2002;8:240–246.
25. Voelkel NF, Tuder RM, Bridges J, Arend WP. Interleukin-1 receptor antagonist treatment reduces pulmonary hypertension generated in rats by monocrotaline. *Am J Respir Cell Mol Biol.* 1994;11:664–675.
26. Kimura H, Kasahara Y, Kurosu K, Sugito K, Takiguchi Y, Terai M, Mikata A, Natsume M, Mukaida N, Matsushima K, Kuriyama T. Alleviation of monocrotaline-induced pulmonary hypertension by antibodies to monocyte chemotactic and activating factor/monocyte chemoattractant protein-1. *Lab Invest.* 1998;78:571–581.
27. Selzman CH, McIntyre RC Jr, Shames BD, Whitehill TA, Banerjee A, Harken AH. Interleukin-10 inhibits human vascular smooth muscle proliferation. *J Mol Cell Cardiol.* 1998;30:889–896.
28. Morrell NW, Yang X, Upton PD, Jourdan KB, Morgan N, Sheares KK, Trembath RC. Altered growth responses of pulmonary artery smooth muscle cells from patients with primary pulmonary hypertension to transforming growth factor-β_1 and bone morphogenetic proteins. *Circulation.* 2001;104:790–795.
29. Botney MD, Bahadori L, Gold LI. Vascular remodeling in primary pulmonary hypertension. Potential role for transforming growth factor-β. *Am J Pathol.* 1994;144:286–295.
30. Tanaka Y, Schuster DP, Davis EC, Patterson GA, Botney MD. The role of vascular injury and hemodynamics in rat pulmonary artery remodeling. *J Clin Invest.* 1996;98:434–442.
31. El-Haroun H, Bradbury D, Clayton A, Knox AJ. Interleukin-1β, transforming growth factor-β_1, and bradykinin attenuate cyclic AMP production by human pulmonary artery smooth muscle cells in response to prostacyclin analogues and prostaglandin E2 by cyclooxygenase-2 induction and downregulation of adenylyl cyclase isoforms 1, 2, and 4. *Circ Res.* 2004;94:353–361.
32. Suzuki C, Takahashi M, Morimoto H, Izawa A, Ise H, Hongo M, Hoshikawa Y, Ito T, Miyashita H, Kobayashi E, Shimada K, Ikeda U. Mycophenolate mofetil attenuates pulmonary arterial hypertension in rats. *Biochem Biophys Res Commun.* 2006;349:781–788.
33. Minamino T, Christou H, Hsieh CM, Liu Y, Dhawan V, Abraham NG, Perrella MA, Mitsialis SA, Kourembanas S. Targeted expression of heme oxygenase-1 prevents the pulmonary inflammatory and vascular responses to hypoxia. *Proc Natl Acad Sci U S A.* 2001;98:8798–8803.

THE JOURNAL OF BIOLOGICAL CHEMISTRY VOL. 282, NO. 36, pp. 26369–26380, September 7, 2007

Soluble ST2 Blocks Interleukin-33 Signaling in Allergic Airway Inflammation*[S]

Received for publication, June 14, 2007, and in revised form, June 29, 2007 Published, JBC Papers in Press, July 10, 2007, DOI 10.1074/jbc.M704916200

Hiroko Hayakawa[‡], Morisada Hayakawa[‡1], Akihiro Kume[§], and Shin-ichi Tominaga[‡]

From the [‡]Department of Biochemistry and [§]Division of Genetic Therapeutics, Jichi Medical University, 3311-1 Yakushiji, Shimotsuke-shi, Tochigi 329-0498, Japan

The ST2 gene produces a soluble secreted form and a transmembrane form, referred to as soluble ST2 and ST2L, respectively. A recent study has reported that interleukin (IL)-33 is a specific ligand of ST2L and induces production of T helper type 2 (Th2) cytokines. Although soluble ST2 is highly produced in sera of asthmatic patients and plays a critical role for production of Th2 cytokines, the function of soluble ST2 in relation to IL-33 signaling remains unclear. Here we show antagonistic effects of soluble ST2 on IL-33 signaling using a murine thymoma EL-4 cells stably expressing ST2L and a murine model of asthma. Soluble ST2 directly bound to IL-33 and suppressed activation of NF-κB in EL-4 cells stably expressing ST2L, suggesting that the complex of soluble ST2 and IL-33 fails to bind to ST2L. In a murine model of asthma, pretreatment with soluble ST2 reduced production of IL-4, IL-5, and IL-13 from IL-33-stimulated splenocytes. These results indicate that soluble ST2 acts as a negative regulator of Th2 cytokine production by the IL-33 signaling. Our study provides a molecular mechanism wherein soluble ST2 modulates the biological activity of IL-33 in allergic airway inflammation.

The interleukin (IL)-1[2] receptor family plays important roles in inflammatory and immunological responses. The ST2 gene is a member of the IL-1 receptor family, producing a soluble secreted form and a transmembrane form, soluble ST2 and ST2L, respectively (1–3). These proteins are generated by alternative splicing of pre-mRNA. The structure of ST2L is similar to that of IL-1 receptor type I (IL-1RI), consisting of three extracellular immunoglobulin domains and an intracellular Toll-interleukin-1 receptor domain. Although the extracellular domain is common to soluble ST2 and ST2L, soluble ST2 lacks the transmembrane and intracellular Toll-interleukin-1 receptor domains. The ST2 gene is expressed in several cells including fibroblasts and mast cells (1, 4). In particular, ST2L is preferentially expressed in murine and human Th2 cells and can be utilized as a specific marker of Th2 cells in *in vitro* experiments (5–8). Therefore, the function of ST2L has been suggested to correlate with Th2 cell-mediated immunological responses. However, ST2L has been an orphan receptor ever since it was first reported (5). Late in 2005, IL-33, a newly discovered member of the IL-1 cytokine family, was finally reported as a specific ligand for ST2L (9).

The IL-33 gene, also described as a nuclear factor expressed in high endothelial venules (NF-HEV) (10), codes a 31-kDa protein that does not contain a signal sequence for secretion, similar to the IL-1α, IL-1β, and IL-18 genes (11, 12). Previous study has demonstrated the processing and function of the IL-33 protein (9). The precursor 31-kDa protein (pre-IL-33) was cleaved by caspase-1 into a mature 18-kDa protein (IL-33) in *in vitro* experiments using a recombinant protein. Functional analysis has shown that IL-33 bound to murine mast cells expressing ST2L and stimulated the intracellular signaling pathway, leading to the activation of NF-κB and mitogen-activated protein kinases. In addition, the production of Th2 cytokines and severe pathological changes in mucosal organs were induced by administration of IL-33 to mice. Previous studies before the discovery of IL-33 had already shown that ST2L is associated with the production of Th2 cytokines. Levels of Th2 cytokines were decreased in asthmatic mice by administration of the antibody that blocks ST2L and in a pulmonary granuloma model using mice lacking the ST2 gene (7, 13). Therefore, these results suggest that IL-33 signaling via ST2L plays important roles in Th2 cell-mediated immunological responses including the production of Th2 cytokines.

On the other hand, previous studies in human patients and animal models have shown that the level of soluble ST2 in sera was elevated in asthmatic disease (14, 15). Therefore, it has been suggested that soluble ST2 may also play a critical role in Th2 cell-mediated diseases. In fact, administration of a recombinant soluble ST2-Fc fusion protein or a soluble ST2 expression vector to asthmatic mice effectively attenuated inflammatory responses and production of Th2 cytokines (7, 15). These results of therapeutic experiments indicate that soluble ST2 negatively regulates the Th2 cell-mediated immunological responses, in opposition to ST2L. However, the molecular mechanism of negative regulation by soluble ST2 remains unclear. In addition, it has not been addressed whether soluble ST2 is associated with IL-33 signaling.

In this study, using a murine thymoma cell line, EL-4, stably expressing ST2L and a murine model of asthma, we demonstrated that soluble ST2 had a negative function in IL-33 signal-

* This work was supported by a Grant-in-Aid from the Ministry of Education, Culture, Sports, Science and Technology of Japan. The costs of publication of this article were defrayed in part by the payment of page charges. This article must therefore be hereby marked "*advertisement*" in accordance with 18 U.S.C. Section 1734 solely to indicate this fact.

[S] The on-line version of this article (available at http://www.jbc.org) contains supplemental Figs. S1 and S2.

[1] To whom correspondence should be addressed. Tel.: 81-285-58-7324; Fax: 81-285-44-2158; E-mail: morisada@jichi.ac.jp.

[2] The abbreviations used are: IL, interleukin; Th, T helper; IFN-γ, interferon-γ; OVA, ovalbumin; NF-κB, nuclear factor-κB; IκB, inhibitor of NF-κB; PBS, phosphate-buffered saline; FITC, fluorescein isothiocyanate; RPE, R-phycoerythrin; EMSA, electrophoretic mobility shift assay; ELISA, enzyme-linked immunosorbent assay; SAL, saline.

ing. Binding and functional analyses showed that soluble ST2 inhibited the binding of IL-33 to ST2L-positive cells and that the activation of NF-κB and the production of Th2 cytokines in the IL-33 signaling were suppressed in the presence of soluble ST2. Our data suggest that soluble ST2 negatively modulates the production of Th2 cytokines through IL-33 signaling in allergic airway inflammation.

EXPERIMENTAL PROCEDURES

Animals—Male and female BALB/c mice, 7–8 weeks of age, were purchased from Japan SLC, Inc. (Shizuoka, Japan). All of the mice were housed in an animal research facility of the Jichi Medical University under pathogen-free conditions. All of the experimental procedures were approved by the Animal Research Ethics Board of Jichi Medical University.

Sensitization and Aeroallergen Challenge—The mice were sensitized by intraperitoneal injection with 100 μg of ovalbumin (OVA) (Sigma-Aldrich) and 20 mg of aluminum potassium sulfate (Sigma-Aldrich) in saline or 20 mg of aluminum potassium sulfate alone in saline on days 0 and 7. On days 14 and 15, the mice were challenged twice daily at intervals of 4 h with 1% (w/v) OVA in saline or saline alone for 30 min using an ultrasonic nebulizer (Omron Corp., Tokyo, Japan) (15). The mice were sacrificed 3–48 h after the last aeroallergen challenge, and sera and tissues were obtained for further analyses. Briefly, blood was drawn from the caudal vena cava and left for 30 min, and then the serum was separated by centrifugation. The sera were stored at −80 °C until assay.

Cell Culture—Human embryonic kidney HEK293T cells were cultured in Dulbecco's modified Eagle's medium (Sigma-Aldrich) supplemented with 10% fetal bovine serum (Thermo Electron, Melbourne, Australia). Murine thymoma EL-4 cells were cultured in RPMI 1640 medium (Sigma-Aldrich) supplemented with 5% fetal bovine serum (Sigma-Aldrich) and 50 μM 2-mercaptoethanol (RPMI 1640 growth medium).

Reverse Transcription-PCR Analysis—Total RNAs were isolated from murine tissues using TRI reagent (Sigma-Aldrich). The total RNA was treated with RNase-free DNase I; then first-strand cDNA was synthesized as described previously (16). PCR amplification was performed using 0.5 units of AmpliTaq Gold DNA polymerase (Applied Biosystems, Foster, CA), 0.5 μM each of the forward and reverse primers, and the first-strand cDNAs derived from 0.25 μg of DNase I-treated RNA. After cDNAs were treated at 94 °C for 10 min, PCR was carried out for 25 (β-actin), 28 (IL-33), or 33 (ST2 and ST2L) cycles at 94 °C for 1 min, 60 °C for 1 min, and 72 °C for 1.5 min, followed by treatment at 72 °C for 10 min. The nucleotide sequences of primers used were as follows: ST2, forward 5′-TGGCATGATAAGGCACACCATAAGGCT-3′ and reverse 5′-GTTAGTGTCTCTCTCCCTCCCATGC-3′; ST2L, forward 5′-TGCGTACATCATTTACCCTCGGGTC-3′ and reverse 5′-TCTTGTGCCACAAGAGTGAAGTAGG-3′; IL-33, forward 5′-ATGAGACCTAGAATGAAGTATTCCA-3′ and reverse 5′-TTAGATTTTCGAGAGCTTAAACATA-3′; and β-actin, forward 5′-ATCTACGAGGGCTATGCTCT-3′ and reverse 5′-TACTCCTGCTTGCTGATCCA-3′. Seven microliters of PCR products were developed by electrophoresis on 2% agarose gels, and then the gels were stained with ethidium bromide. The intensity of DNA bands was quantified using the public domain NIH Image program (developed at the United States National Institutes of Health). The size of PCR products was as follows: ST2 (754 bp), ST2L (739 bp), IL-33 (801 bp), and β-actin (576 bp).

Construction of Plasmids—Constructions of pET-21-mIL-33 and pET-21-mIL-1β proceeded as follows. The coding regions of mature IL-33 and IL-1β proteins were obtained from cDNA derived from spleens of BALB/c mice by PCR amplification. The nucleotide sequences of primers containing an EcoRI or an XhoI site were as follows: IL-33, forward 5′-GAATTCACATTGAGCATCCAAGGAAC-3′ and reverse 5′-CTCGAGGATTTTCGAGAGCTTAAACA-3′; IL-1β, forward 5′-GAATTCGTTCCCATTAGACAGCTGCA-3′ and reverse 5′-CTCGAGGGAAGACACAGATTCCATGG-3′. PCR products were digested with EcoRI and XhoI and then ligated into an EcoRI/XhoI-digested pET-21a (+) vector (Novagen, Madison, WI). Expression vectors of murine soluble ST2 were constructed using pEF6-V5-His (Invitrogen) and pEF6-FLAG-His. Construction of pEF6-FLAG-His proceeded as follows. A fragment containing FLAG and His tags (FLAG-His) was created by annealing a sense oligonucleotide (5′-GCGGCCGCTGACTACAAGGATGACGATGACAAGCGTACCGGTC-3′) and an antisense oligonucleotide (5′-GTTTAAACTCAATGGTGATGGTGATGATGACCGGTACGCTTGT-3′), and the annealed fragment was elongated and subcloned into a pCR2.1 TOPO (Invitrogen). A NotI/PmeI-digested FLAG-His fragment was ligated into a NotI/PmeI-digested pEF6-V5-His. Murine ST2 (mST2) cDNA was amplified from pEF-BOS-mST2 (17) by PCR using a forward primer containing a KpnI site (5′-GGTACCATGATTGACAGACAGAGAAT-3′) and a reverse primer containing a NotI site (5′-GCGGCCGCAGCAATGTGTGAGGGACACT-3′). A KpnI/NotI-digested PCR product was ligated into a KpnI/NotI-digested pEF6-V5-His and pEF6-FLAG-His to obtain final products pEF6-mST2-V5-His and pEF6-mST2-FLAG-His, respectively. Constructions of pEF6-mST2L-FLAG and pEF6-mIL-1RI-FLAG proceeded as follows. Murine ST2L (mST2L) cDNA was amplified from pEF-BOS-mST2L (5) by PCR using a forward primer containing a BamHI site (5′-GGATCCATGATTGACAGACAGAGA-3′) and a reverse primer containing a NdeI site (5′-CATATGAAAGTGTTTCAGGTCTAA-3′). The PCR product was subcloned into a pCR2.1 TOPO (pCR2.1-mST2L). A FLAG fragment containing a stop codon was created by annealing FLAG-s (5′-TATGGATTACAAGGATGACGACGATAAGTAGA-3′) and FLAG-as (5′-CTAGTCTACTTATCGTCGTCATCCTTGTAATCCA-3′), and the annealed fragment was ligated into a NdeI/SpeI-digested pCR2.1-mST2L. Finally, the mST2L-FLAG fragment was digested with BamHI and SpeI and ligated into a BamHI/SpeI-digested pEF6/V5-His. Murine IL-1RI (mIL-1RI) cDNA was obtained from cDNA derived from EL-4 cells by PCR amplification using primers containing a KpnI or a NdeI site (forward 5′-GGTACCATGGAGAATATGAAAGTGCTA-3′ and reverse 5′-CATATGGCCGAGTGGTAAGTGTGTTGC-3′). Murine ST2L cDNA in pEF6-mST2L-FLAG was replaced with mIL-1RI cDNA, using KpnI and NdeI digestion. All of the constructs were confirmed to be correct by DNA sequencing analysis.

Purification of Recombinant IL-33 and IL-1β Proteins—Recombinant murine IL-33 and IL-1β proteins containing a T7 tag at the N terminus and a His tag at the C terminus (rIL-33 and rIL-1β) were produced in bacteria. BL-21 Codon-Plus (DE3)-RIL (Stratagene, La Jolla, CA) was transformed with pET-21-mIL-33 or pET-21-mIL-1β. The bacteria were cultured at 37 °C until the A_{600} reached 0.6; then expression of recombinant protein was induced by the addition of isopropyl β-D-thiogalactopyranoside to a final concentration of 1 mM. Three hours after culture at 25 °C, the bacteria were harvested, and the pellets were resuspended in lysis buffer (50 mM Na_2HPO_4, 300 mM NaCl, 10 mM imidazole) containing 1 mg/ml lysozyme. After sonication, the soluble cytoplasmic fraction was isolated by centrifugation. The fraction was loaded onto a nickel-nitrilotriacetic acid-agarose (Qiagen) column. The proteins were eluted with elution buffer (50 mM Na_2HPO_4, 300 mM NaCl, 250 mM imidazole). After dialysis against T7 tag binding buffer (4.3 mM Na_2HPO_4, 1.5 mM KH_2PO_4, 2.7 mM KCl, 137 mM NaCl, 0.1% (v/v) Tween 20, pH 7.3), the proteins were purified using a T7 tag affinity purification kit (Novagen). The proteins were eluted from the column with 0.1 M citric acid (pH 2.2) and neutralized with 2 M Tris base (pH 10.4). After desalting and concentrating the protein using Centricon YM-3 (Millipore, Bedford, MA), the purified proteins were dialyzed against PBS (8 mM Na_2HPO_4, 1.5 mM KH_2PO_4, 2.7 mM KCl, 137 mM NaCl). The protein concentration was determined by the Bradford method using protein assay dye reagent (Bio-Rad) with calibration using bovine serum albumin (Sigma-Aldrich). The protein purity was evaluated using a silver staining kit (Daiichi Pure Chemicals, Tokyo, Japan).

Purification of Recombinant Soluble ST2 Proteins—Recombinant soluble ST2 proteins containing V5-His or FLAG-His tags at the C terminus (ST2-V5 and ST2-FLAG) were purified as described previously (18). Briefly, HEK293T cells were transiently transfected with pEF6-mST2-V5-His or pEF6-mST2-FLAG-His using the calcium-phosphate method. Sixteen hours after transfection, the cells were cultured in serum-free Dulbecco's modified Eagle's medium for 48 h. The secreted recombinant proteins in the culture supernatant were purified by affinity chromatography using nickel-nitrilotriacetic acid-agarose (Qiagen). The proteins were eluted with 50 mM sodium phosphate buffer (pH 8.0) containing 300 mM NaCl and 250 mM imidazole. Desalting and concentrating the proteins were performed using Centricon YM-30 (Millipore). Finally, the purified proteins were dialyzed against PBS. The method for measuring the protein concentration is described under "Measurement of Soluble ST2 and Cytokines." Deglycosylation with *N*-glycosidase F (Roche Applied Science) was performed as described previously (17). The protein purity was evaluated using a silver staining kit.

Establishment of Stable Cell Lines—Empty vector (pEF6-V5-His) and expression vectors (pEF6-mST2L-FLAG and pEF6-mIL-1RI-FLAG) were linearized with FspI. EL-4 cells (1×10^7 cells) were mixed with 50 μg of linearized plasmid DNA in serum-free RPMI 1640 medium, and the mixtures were left for 10 min on ice. Electroporation was carried out using a Gene Pulser (Bio-Rad) at 270 V and 960 microfarads, and then the cells were left on ice for 10 min. The transfected cells were returned to the RPMI 1640 growth medium and were incubated at 37 °C in 5% CO_2. Forty-eight hours after transfection, the transfected cells were selected with blasticidin (Invitrogen). Stable clones were cultured in RPMI 1640 growth medium containing 6 μg/ml blasticidin.

Flow Cytometry—Splenocytes (1×10^6 cells) and stably transfected EL-4 cells (5×10^5 cells) were used for flow cytometric analysis. Preparation of splenocytes proceeded as follows. The spleen was homogenized into a single-cell suspension in PBS by filtration through nylon mesh (70 μm). After depletion of erythrocytes by osmotic lysis, the splenocytes were washed with PBS and resuspended in PBS containing 5% fetal bovine serum. Subsequently, anti-mouse CD16/CD32 antibody (BD Biosciences PharMingen, San Diego, CA) was mixed with the splenocytes to block the Fc receptor for 5 min on ice. Binding analysis of IL-33 and IL-1β on the cell surface was performed as follows. The cells were mixed with 100 or 500 ng of rIL-33 or rIL-1β for 1 h on ice, followed by staining with biotinylated anti-T7 tag antibody (Novagen) for 1 h on ice. Then the cells were stained with R-phycoerythrin (RPE)-conjugated streptavidin (DakoCytomation, Glostrup, Denmark) for 30 min on ice. In case of binding analysis in the presence of soluble ST2, 1 μg of ST2-V5 was added to the cells at 1 h before, at 1 h after, or at the same time as the addition of rIL-33 or rIL-1β. Binding of ST2-V5 was detected with fluorescein isothiocyanate (FITC)-conjugated anti-V5 antibody (Invitrogen) for 1 h on ice. ST2L or IL-1RI was stained with FITC-conjugated anti-mouse T1/ST2 antibody (MD Biosciences, Zürich, Switzerland), RPE-conjugated anti-mouse IL-1RI antibody (BD Biosciences PharMingen), or each isotype control antibody for 1 h on ice. After the stained cells were washed twice with PBS containing 5% fetal bovine serum, the cells were resuspended in PBS and filtered through nylon mesh (35 μm). Analysis was performed on Becton Dickinson LSR using Cell Quest software (BD Biosciences).

Immunoprecipitation—Five hundred ng of ST2-V5 was mixed with 2 μg of rIL-33 or rIL-1β in 500 μl of RIPA buffer (50 mM Tris-HCl, pH 8.0, 150 mM NaCl, 1% (v/v) Nonidet P-40, 0.5% (w/v) deoxycholate, 0.1% (w/v) SDS), and the mixture was agitated overnight at 4 °C. The protein complexes were immunoprecipitated with 40 μl of 50% (v/v) slurry of anti-T7 tag antibody-conjugated agarose (Novagen). After the protein-bound agarose was washed three times with RIPA buffer, binding protein complexes were eluted with 0.1 M citric acid (pH 2.2) and neutralized with the addition of 2 M Tris (pH 10.4). The eluted proteins were subjected to Western blotting.

Western Blotting—The protein samples were separated by electrophoresis on SDS-polyacrylamide gels. The proteins were transferred to a polyvinylidene difluoride membrane (Millipore) and were probed with mouse monoclonal anti-T7 tag (Novagen), rabbit polyclonal anti-IL-33 (Adipogen Inc., Seoul, South Korea), goat polyclonal anti-IL-1β (Santa Cruz Biotechnology, Santa Cruz, CA), mouse monoclonal anti-V5 (Invitrogen), mouse monoclonal anti-His (C Term) (Invitrogen), rabbit polyclonal anti-IκBα (Santa Cruz), or mouse monoclonal anti-glyceraldehyde-3-phosphate dehydrogenase (Santa Cruz) antibody as the primary antibody. The proteins were detected with

horseradish peroxidase-conjugated goat anti-mouse Ig (Bio-Rad), horseradish peroxidase-conjugated horse anti-goat Ig (Vector, CA), or horseradish peroxidase-conjugated donkey anti-rabbit Ig (Amersham Biosciences) as the secondary antibody. The proteins were visualized using Immobilon Western detection reagents (Millipore), and the membranes were exposed to x-ray films (RX-U; Fuji Photo Film Co., Tokyo, Japan).

Preparation of Cytoplasmic and Nuclear Extracts—Preparation of cytoplasmic and nuclear extracts from stably transfected EL-4 cells was performed as described previously (16). Briefly, the cells were harvested and rinsed with PBS. The cell pellets were resuspended in 5 volumes of a buffer solution (10 mM Hepes-KOH, pH 8.0, 10 mM KCl, 1.5 mM $MgCl_2$, 1 mM dithiothreitol). After addition of Nonidet P-40 to a final concentration of 0.1% (v/v), cytoplasmic extracts were separated by centrifugation. The nuclei were resupended in 2.5 volumes of a buffer solution (20 mM Hepes-KOH, pH 8.0, 420 mM KCl, 1.5 mM $MgCl_2$, 0.2 mM EDTA, 25% (v/v) glycerol, 1 mM dithiothreitol, 0.5 mM phenylmethylsulfonyl fluoride) and mixed by agitation. The debris was removed by centrifugation, and the supernatants were dialyzed against a buffer solution (20 mM Hepes, pH 8.0, 100 mM KCl, 0.2 mM EDTA, 20% (v/v) glycerol, 1 mM dithiothreitol, 0.5 mM phenylmethylsulfonyl fluoride). After centrifugation, the supernatants were harvested as nuclear extracts. The protein concentration was determined by the Bradford method. Cytoplasmic and nuclear extracts were stored at −80 °C until assay.

Electrophoretic Mobility Shift Assay (EMSA)—EMSA was performed as described previously, with some modifications (16, 19). Binding reactions were performed at 30 °C for 30 min in a total volume of 15 μl containing nuclear extracts (5 μg of protein) and 20,000 cpm of ^{32}P-labeled oligonucleotide probe. Supershift assay was carried out using antibodies against p50, p52, p65, and c-Rel (Santa Cruz). The protein-DNA complexes were separated on 4% nondenaturing polyacrylamide gels at 100 V in 0.5 × TGE (50 mM Tris-HCl, pH 8.0, 380 mM glycine, 2 mM EDTA) at 4 °C. The dried gels were exposed to Imaging plates (Fuji Photo Film Co.) and analyzed using Typhoon 9410 (Amersham Biosciences). The oligonucleotide probe containing an NF-κB binding site was created by annealing NF-κB-s (5′-AGTTGAGGGGACTTTCCCAGGC-3′) and NF-κB-as (5′-AGCCTGGGAAAGTCCCCTCAAC-3′).

Luciferase Assay—The luciferase assay was performed as described previously (16). EL-4 cells stably expressing ST2L or IL-1RI (1×10^7 cells) were transfected with plasmid DNAs (40 μg of firefly luciferase reporter plasmid, pNF-κB-Luc, containing an NF-κB binding site in the promoter, and 4 μg of the *Renilla* luciferase reporter plasmid pRL-TK (Promega, Madison, WI)) by electroporation. Twenty-four hours after transfection, the cells were washed and cultured in serum-free medium for 15 h. The transfected cells were treated with 500 ng/ml of ST2-V5 for 3 h, followed by stimulation with 10 ng/ml rIL-33 or rIL-1β for 24 h. Then the cells were harvested and subjected to luciferase assay using a dual luciferase reporter assay system (Promega). Luciferase activity was measured by a luminometer (Lumat LB9507; Berthold Technologies, Bad Wildbad, Germany). The firefly luciferase activity was normalized against the respective *Renilla* luciferase activity.

Stimulation of Splenocytes—Splenocytes were prepared as described under "Flow Cytometry" and resuspended in RPMI 1640 growth medium. Splenocytes (4×10^7 cells/well) were stimulated with 200 μg/ml OVA for 48 h in 6-well plate. The OVA-stimulated cells were washed with PBS and resuspended with serum-free RPMI 1640 medium at 2.5×10^6 cells/well in 48-well plate. After incubation for 15 h, ST2-FLAG was added to a final concentration of 500 ng/ml for 3 h. Then the cells were stimulated with 10 ng/ml rIL-33 or rIL-1β for 48 h. The culture supernatant was harvested and stored at −80 °C until assay.

Measurement of Soluble ST2 and Cytokines—The concentrations of soluble ST2 in sera and purified recombinant proteins were measured by a sandwich enzyme-linked immunosorbent assay (ELISA) as described previously (15). The concentrations of IL-4, IL-5, IL-13, and IFN-γ in culture supernatants were measured using ELISA kits (BIOSOURCE International Inc., Camarillo, CA).

Statistical Analysis—The data are represented as the means ± S.E. The data were analyzed by the Turkey-Kramer test. A value of $p < 0.05$ was considered to be significant.

RESULTS

Specific Binding of IL-33 to ST2L-positive Cells—To study the binding and function of IL-33, we developed systems for the expression and purification of mature IL-33 as a recombinant protein (designated as rIL-33) (Fig. 1*A*). In this study, recombinant mature IL-1β (designated as rIL-1β) was also used for control experiments, because IL-1β has binding activity for IL-1RI, but not for ST2L. Recombinant IL-33 and IL-1β containing T7 and His tags were expressed in bacteria and subjected to affinity purification. The purities of rIL-33 and rIL-1β proteins were examined by silver staining and Western blotting (Fig. 1*A*, *a* and *b*). Although rIL-33 was purified as a single band, the purification product of rIL-1β contained a cleaved product. Next, to establish a clear analysis system for the binding of IL-33, we generated cell lines stably expressing ST2L or IL-1RI using EL-4 cells (Fig. 1*B*). Although ST2L was hardly detected in cells stably transfected with an empty vector (EV/EL-4) or an IL-1RI expression vector (IL-1RI/EL-4), remarkable expression of ST2L was observed in ST2L expression vector-transfected cells (ST2L/EL-4). In addition to a constitutive expression of IL-1RI in EL-4 cells, IL-1RI was further expressed in IL-1RI/EL-4 cells. We examined the binding activity of IL-33 using these stably transfected cell lines (Fig. 1*C*). The ST2L/EL-4 cells clearly shifted according to the increasing concentration of rIL-33 (Fig. 1*C*, *middle panel*). Conversely, EV/EL-4 and IL-1RI/EL-4 cells showed little change corresponding to the expression of ST2L. These results demonstrate that IL-33 specifically binds to ST2L.

Inhibition of IL-33 Binding Activity by Soluble ST2—The amino acid sequence of soluble ST2 except for 9 amino acids in the C terminus is the same as that of the extracellular domain of ST2L (1, 3). Therefore, it seemed possible that soluble ST2 might also bind to IL-33. To investigate this possibility, we generated recombinant soluble ST2 containing either V5 or FLAG and His tags in the C terminus (designated as ST2-V5 or ST2-

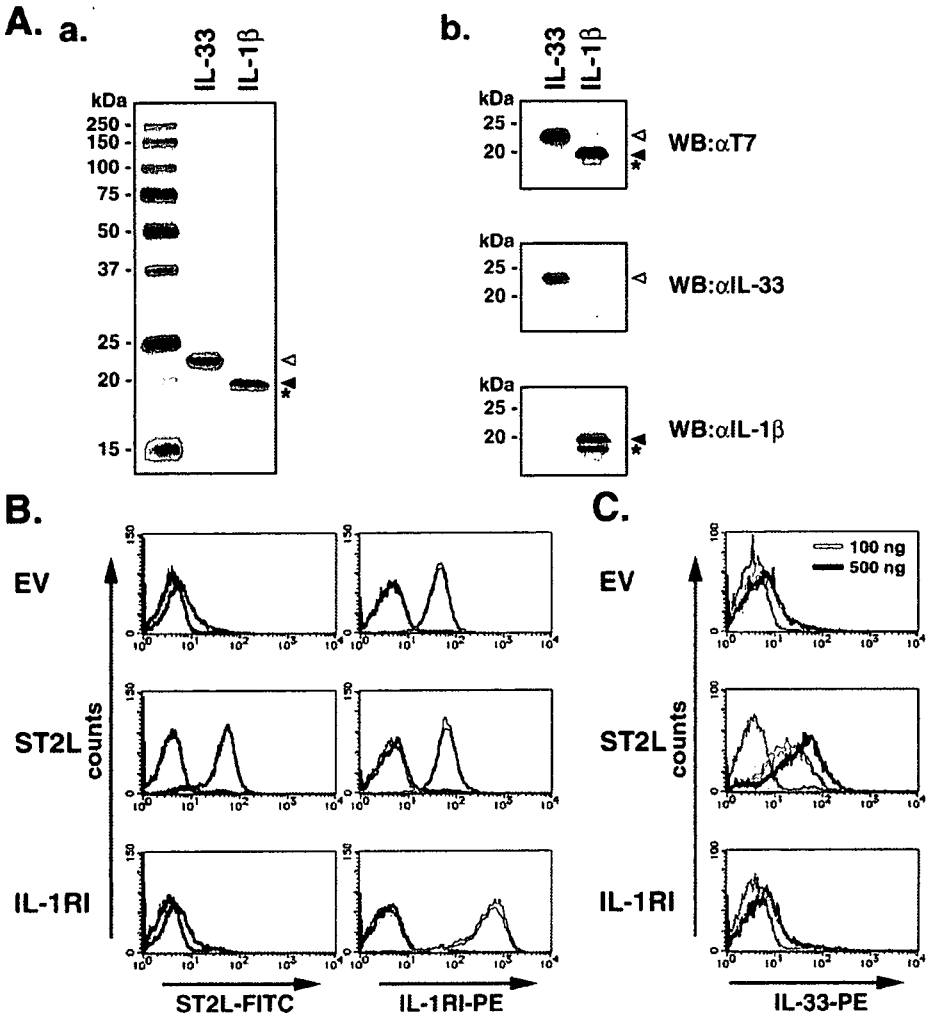

FIGURE 1. **Binding analysis of IL-33 to ST2L-positive cells.** *A*, analysis of purified rIL-33 and rIL-1β. Purified proteins (100 ng) were separated on SDS-12.5% polyacrylamide gels, followed by silver staining (*panel a*) and Western blotting (*WB*) with anti-T7 tag (*αT7*), anti-mouse IL-33 (*αIL-33*), and anti-mouse IL-1β (*αIL-1β*) antibodies (*panel b*). *White* and *black arrowheads* indicate rIL-33 and rIL-1β, respectively. An *asterisk* indicates a cleaved product of rIL-1β. Protein size is indicated in kDa at the *left*. *B*, expression analysis of ST2L and IL-1RI in EL-4 cells. Stably transfected EL-4 cells were generated by introduction of an empty vector, an ST2L expression vector, or an IL-1RI expression vector (*EV*, *ST2L*, or *IL-1RI*). Stably transfected EL-4 cells (5×10^5 cells) were stained with FITC-conjugated anti-mouse T1/ST2 antibody (*magenta line*), RPE-conjugated anti-mouse IL-1RI antibody (*green line*), or each isotype control antibody (*purple line*). The *gray-filled histogram* shows unstained cells. *C*, binding analysis of rIL-33 to EL-4 cells. Stably transfected EL-4 cells (5×10^5 cells) were mixed with 100 ng (*blue line*) or 500 ng (*red line*) of rIL-33 for 1 h. Binding of rIL-33 was detected with biotinylated anti-T7 tag antibody and RPE-conjugated streptavidin. The *gray-filled histogram* shows unstained cells. *B* and *C*, the data of clone numbers 1-1-A-3 (EV/EL-4 cells), 1-2-G-12 (ST2L/EL-4 cells), and 3-2-A-8 (IL-1RI/EL-4 cells) are represented in each figure.

FLAG). Recombinant soluble ST2, expressed in HEK293T cells and secreted into the culture supernatant, was affinity-purified. The purity was confirmed by silver staining (Fig. 2*A*). SDS-PAGE analysis showed that purified recombinant soluble ST2 was detected as a single broad band of 55–65 kDa because of *N*-linked glycosylation. After deglycosylation with *N*-glycosidase F, the molecular mass shifted to 37 kDa, corresponding to an unmodified form. We tested whether soluble ST2 directly interacted with IL-33 *in vitro* (Fig. 2*B*). ST2-V5 was mixed with either rIL-33 or rIL-1β, and protein complexes were immunoprecipitated with anti-T7 tag antibody-conjugated agarose and then eluted from agarose. The eluates were analyzed by Western blotting using anti-V5 and anti-T7 tag antibodies. Analysis of input was performed using the anti-His antibody because both recombinant proteins were His-tagged. These experiments clearly revealed that ST2-V5 specifically bound to rIL-33 but not to rIL-1β (Fig. 2*B*, compare *lanes 3–5*).

To further study the interaction between soluble ST2 and IL-33, we analyzed the binding of rIL-33 to ST2L/EL-4 cells or rIL-1β to IL-1RI/EL-4 cells in the presence of ST2-V5 (Fig. 2*C*). Stably transfected EL-4 cells were either left untreated or treated with ST2-V5 and then added with either rIL-33 or rIL-1β. ST2-V5 inhibited the binding of rIL-33 to ST2L/EL-4 cells (Fig. 2*C*, *upper panel*). In contrast, rIL-1β binding activity for IL-1RI/EL-4 cells was not affected in the presence of ST2-V5 (Fig. 2*C*, *lower panel*). Next, we examined whether the additive order of soluble ST2 influences the binding activity of IL-33 (Fig. 2*D*). ST2-V5 was added to ST2L/EL-4 cells before, after, or at the same time as the addition of rIL-33. When rIL-33 was added prior to ST2-V5, the binding of IL-33 was hardly influenced by the treatment with ST2-V5 (Fig. 2*D*, compare *panels c* and *d*). On the other hand, the binding of IL-33 was inhibited by the treatment with ST2-V5 at the same time or before the addition of rIL-33 (Fig. 2*D*, compare *panels c*, *e*, and *f*). In addition, the binding of ST2-V5 to ST2L/EL-4 cells was not observed regardless of the binding of IL-33 in this system. These results indicate that soluble ST2 specifically binds to free IL-33 and inhibits the binding activity of IL-33 for ST2L and that the ST2/IL-33 complex cannot bind to ST2L-positive cells.

Suppression of IL-33-induced NF-κB Activation by Soluble ST2—To study the activation of NF-κB by IL-33 signaling, we examined the DNA binding activity of NF-κB by EMSA and the degradation of IκBα by Western blotting (Fig. 3*A* and supplemental Fig. S1). Nuclear and cytoplasmic extracts were prepared from rIL-33- or rIL-1β-stimulated EL-4 cells. EMSA clearly showed that intracellular responses in the IL-33 and IL-1β signalings were consistent with the expression of ST2L and IL-1RI, respectively. Stimulation with rIL-33 specifically induced the DNA binding activity of NF-κB (Fig. 3*A*, *panel a*, *lane 6*) and the degradation of IκBα (Fig. 3*A*, *panel b*, *lane 5*) in ST2L-EL-4 cells. On the other hand, stimulation with rIL-1β

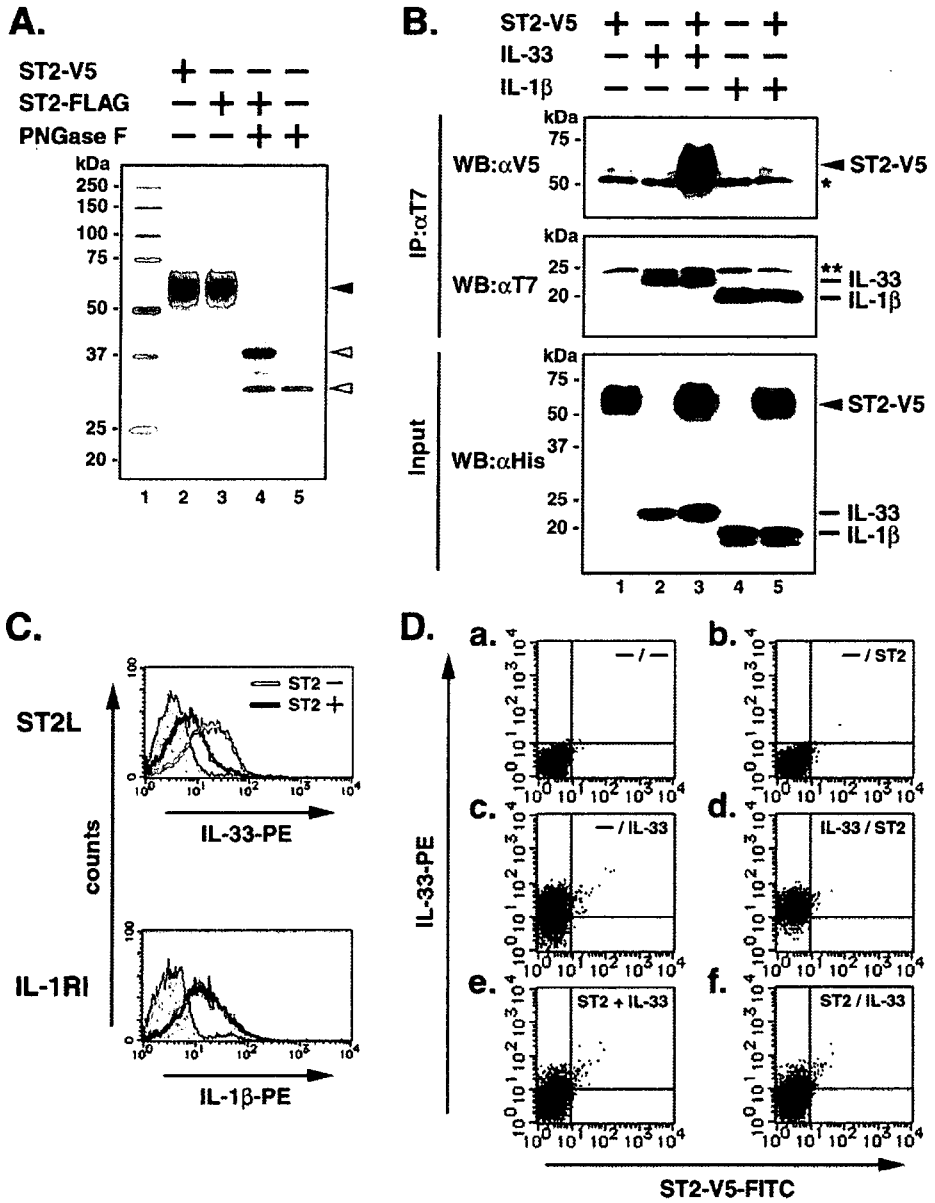

FIGURE 2. **Binding analysis of soluble ST2 to IL-33.** *A*, analysis of purified recombinant soluble ST2. Purified ST2-V5 and ST2-FLAG (100 ng) were left untreated or treated with *N*-glycosidase F. The proteins were separated on SDS-10% polyacrylamide gel, followed by silver staining. Glycosylated and deglycosylated proteins are indicated by *black* and *gray arrowheads*, respectively. *N*-Glycosidase F (*PNGase F*) is indicated by a *white arrowhead*. *B*, analysis of interaction between ST2-V5 and rIL-33, or rIL-1β. ST2-V5 (500 ng) was mixed with rIL-33 or rIL-1β (2 μg) in RIPA buffer. The protein complexes were immunoprecipitated with anti-T7 tag antibody-conjugated agarose (*IP: αT7*). The proteins were eluted with 0.1 M citric acid (pH 2.2) and neutralized with 2 M Tris (pH 10.4), followed by Western blotting (*WB*) with anti-V5 (*αV5*) and anti-T7 tag (*αT7*) antibodies. Input was analyzed by Western blotting with anti-His antibody (*αHis*) using 1/20 volumes of reaction mixture. *Single* and *double asterisks* indicate heavy and light chains of immunoglobulin, respectively. *A* and *B*, protein size is indicated in kDa at the *left*. *C*, effect of ST2-V5 on binding activity of rIL-33 or rIL-1β. Stably transfected EL-4 cells (5 × 10^5 cells) were either left untreated or treated with ST2-V5 (1 μg) for 1 h, and then rIL-33 or rIL-1β (100 ng) was admixed for 1 h. Binding of rIL-33 or rIL-1β was detected with biotinylated anti-T7 tag antibody and RPE-conjugated streptavidin. *Upper panel*, binding of rIL-33 to ST2L/EL-4 cells (clone, 1-2-G-12). *Lower panel*, binding of rIL-1β to IL-1RI/EL-4 cells (clone, 3-2-A-8). *Blue-* and *orange-lined histograms* represent cells untreated or treated with ST2-V5, respectively. The *gray-filled histogram* shows unstained cells. *D*, effect of difference of ST2-V5-additive order on IL-33 binding activity. Binding of ST2-V5 was detected with FITC-conjugated anti-V5 antibody. The additive order of proteins was as follows: *panel a*, no addition (−/−); *panel b*, ST2-V5 for 1 h alone (−/ST2); *panel c*, rIL-33 for 1 h alone (−/IL-33); *panel d*, rIL-33 for 1 h prior to ST2-V5 for another 1 h (IL-33/ST2); *panel e*, ST2-V5 and rIL-33 at the same time for 1 h (ST2 + IL-33); *panel f*, ST2-V5 for 1 h prior to rIL-33 for another 1 h (ST2/IL-33).

induced the activation of NF-κB (Fig. 3*A*, *panel a*, *lanes 4*, *7*, and *10*) and the degradation of IκBα (Fig. 3*A*, *panel b*, *lanes 3*, *6*, and *9*) in all cell lines, using constitutively expressed IL-1RI. Next, we investigated components of activated NF-κB using specific antibodies against NF-κB. Supershift assay showed that the p50 and p65 subunits were contained in the IL-33-induced DNA/NF-κB complex (Fig. 3*B*, *lanes 3* and *5*), as well as in the IL-1β-induced DNA/NF-κB complex (Fig. 3*B*, *lanes 8* and *10*).

To further investigate the effect of soluble ST2 on IL-33 signaling, we examined the DNA binding activity of NF-κB and the degradation of IκBα in the presence of soluble ST2 (Fig. 3*C* and supplemental Fig. S2). Stably transfected EL-4 cells were either left untreated or treated with ST2-V5 and then were left unstimulated or stimulated with rIL-33 or rIL-1β. In IL-33-stimulated ST2L/EL-4 cells, the DNA/NF-κB complex was gradually decreased as the concentration of ST2-V5 increased (Fig. 3*C*, *panel a*, *lanes 5–7*). In contrast, pretreatment with ST2-V5 led to the repression of IκBα degradation (Fig. 3*C*, *panel b*, *lanes 4–6*). On the other hand, ST2-V5 did not affect the NF-κB activation and IκBα degradation in the IL-1β signaling (Fig. 3*C*, *panel a*, *lanes 11–13*, and *panel b*, *lanes 10–12*). In addition, we examined NF-κB-dependent luciferase activity in IL-33- or IL-1β-stimulated EL-4 cells (Fig. 3*D*). Stimulation with IL-33 effectively induced NF-κB-dependent luciferase activity in ST2L/EL-4 cells. The IL-33-induced luciferase activity also slightly increased in IL-1RI/EL-4 cells coincident with low expression levels of ST2L. Furthermore, pretreatment with ST2-V5 reduced the IL-33-induced luciferase activities in both cell lines. On the other hand, IL-1β-induced luciferase activities in both cell lines were not affected by the addition of ST2-V5. These results demonstrate that soluble ST2 specifically suppresses the activation of NF-κB by IL-33 signaling via ST2L.

Expression of Soluble ST2 and ST2L in a Murine Model of Asthma—Previous studies have shown that expressions of soluble ST2 and ST2L increased in asthma. To investigate the expressions of soluble ST2 and ST2L

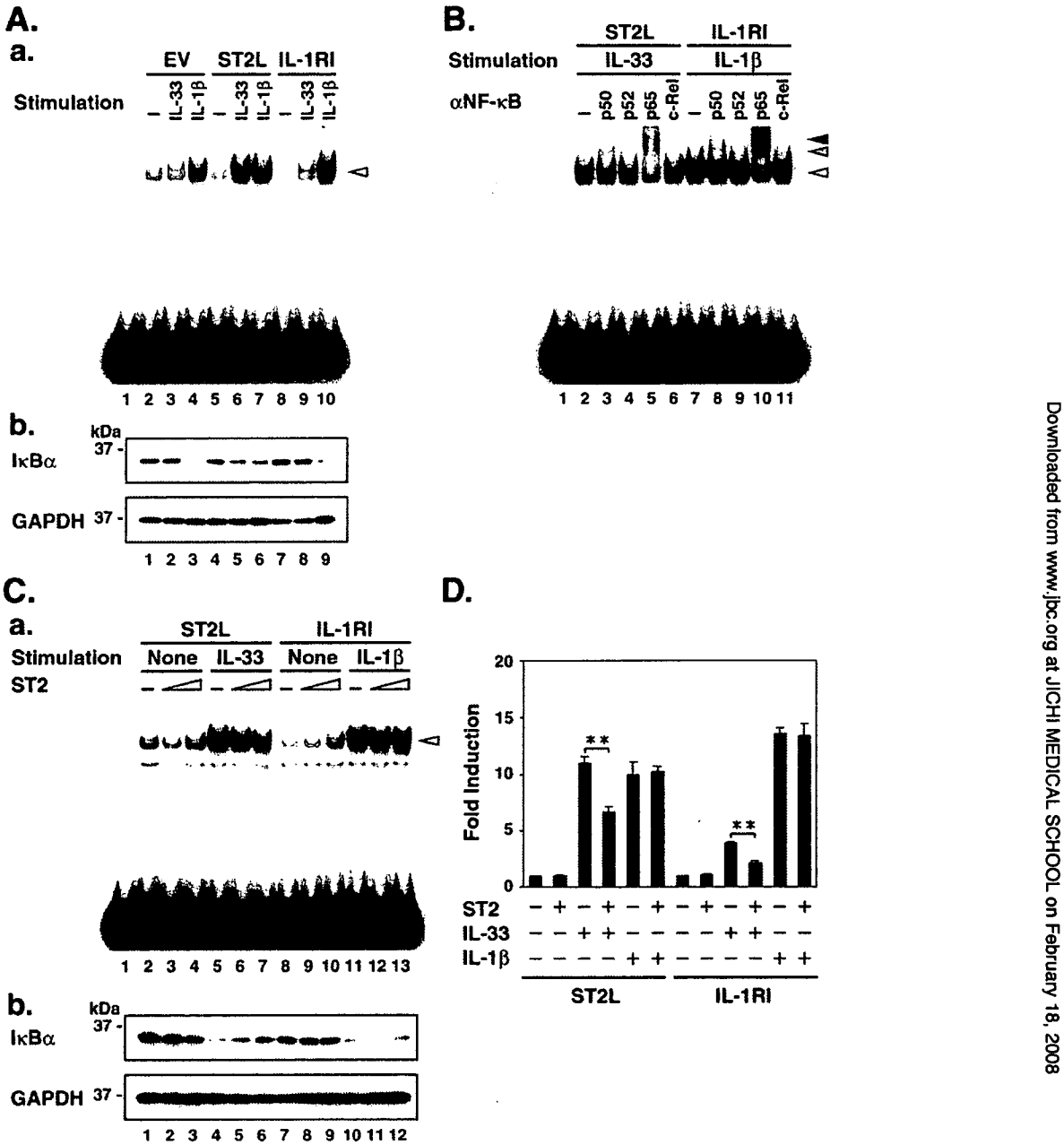

FIGURE 3. **Suppression of IL-33-induced NF-κB activation by soluble ST2.** *A*, analysis of intracellular responses in the IL-33 and IL-1β signalings. Stably transfected EL-4 cells (2×10^7 cells) were either left unstimulated or stimulated with rIL-33 or rIL-1β (10 ng/ml) for 30 min, followed by preparation of cytoplasmic and nuclear extracts. *Panel a*, EMSA using nuclear extracts with a ^{32}P-labeled oligonucleotide probe containing an NF-κB-binding site. The DNA-protein complexes were separated on a 4% nondenaturing polyacrylamide gel. *Panel b*, detection of IκBα and glyceraldehyde-3-phosphate dehydrogenase (*GAPDH*) in cytoplasmic extracts. Cytoplasmic extracts were separated on SDS-12.5% polyacrylamide gels, followed by Western blotting with anti-IκBα and anti-glyceraldehyde-3-phosphate dehydrogenase antibodies. *B*, supershift assay using anti-NF-κB antibodies. Nuclear extracts were kept on ice for 1 h without antibody (*lanes 2* and *7*) or with a series of anti-NF-κB antibodies (*lanes 3–6* and *8–11*), and then the ^{32}P-labeled oligonucleotide probe was admixed. The mixture was kept at 30 °C for 30 min and then subjected to EMSA. *C*, suppression of DNA binding activity of NF-κB by the addition of ST2-V5. Stably transfected EL-4 cells were either left untreated or treated with ST2-V5 (10 and 100 ng) for 3 h and then left unstimulated or stimulated with rIL-33 or rIL-1β for 30 min. After stimulation, cytoplasmic and nuclear extracts were prepared. *Panel a*, DNA binding activity of NF-κB was analyzed by EMSA. *Panel b*, degradation of IκBα was analyzed by Western blotting. *Lanes 1* of *A* (*panel a*), *B*, and *C* (*panel a*) contained the ^{32}P-labeled oligonucleotide probe alone. The DNA/NF-κB and supershifted complexes are indicated by *white*, *gray* (supershifted by αp50), and *black* (supershifted by αp65) *arrowheads*, respectively. *D*, transcriptional activity of rIL-33-or rIL-1β-induced NF-κB. Stably transfected EL-4 cells (1×10^7 cells) were transiently transfected with pNF-κB-Luc (40 μg) and pRL-TK (4 μg). The transfected cells were either left untreated or treated with ST2-V5 (500 ng/ml) for 3 h and then either left unstimulated or stimulated with rIL-33 or rIL-1β (10 ng/ml) for 24 h. The cells were harvested and subjected to luciferase assay. Firefly luciferase activity was normalized with *Renilla* luciferase activity, and the luciferase activity of the untreated and unstimulated cells was given a reference value of 1. The data are shown as the means ± S.E. from four independent experiments. **, $p < 0.01$, IL-33 alone *versus* ST2 plus IL-33). The data of clone numbers 1-1-A-3 (EV/EL-4 cells), 1-2-G-12 (ST2L/EL-4 cells), and 3-2-A-8 (IL-1RI/EL-4 cells) are represented in each panel.

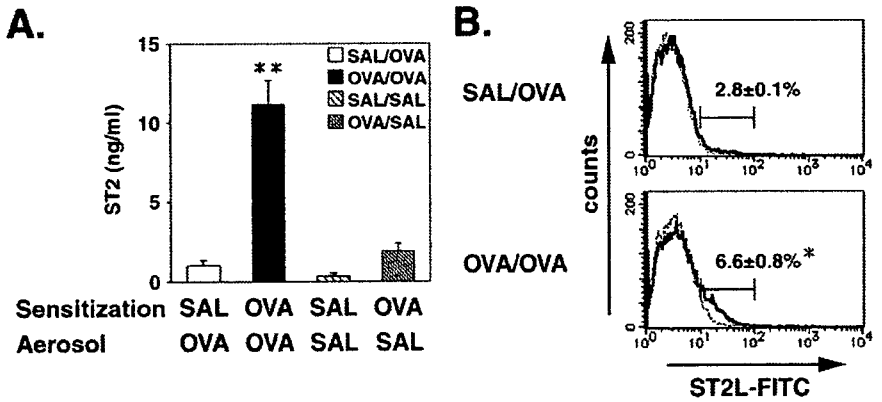

FIGURE 4. **Expression of soluble ST2 and ST2L in a murine model of asthma.** *A*, level of soluble ST2 in sera after aeroallergen challenge. The mice were sensitized with saline and challenged with OVA (*SAL/OVA*), sensitized and challenged with OVA (*OVA/OVA*), sensitized and challenged with saline (*SAL/SAL*), or sensitized with OVA and challenged with saline (*OVA/SAL*). The sera were obtained at 24 h after the last aeroallergen challenge. The concentration of soluble ST2 was measured by sandwich ELISA. The data are shown as the means ± S.E. ($n = 10$ mice/group; **, $p < 0.01$, OVA/OVA *versus* either SAL/OVA, SAL/SAL, or OVA/SAL). *B*, expression analysis of ST2L in splenocytes. Splenocytes were prepared from SAL/OVA and OVA/OVA mice at 24 h after the last OVA challenge. Splenocytes (1×10^6 cells) were stained with FITC-conjugated anti-mouse T1/ST2 antibody (*solid line*) and then analyzed by flow cytometry. The *thin-lined histogram* shows unstained cells. Percentages of ST2L-positive splenocytes are shown as the means ± S.E. ($n = 8$ mice in SAL/OVA, $n = 9$ mice in OVA/OVA; *, $p < 0.05$, OVA/OVA *versus* SAL/OVA).

proteins *in vivo*, we utilized a murine model of asthma caused by OVA. BALB/c mice were sensitized with saline (SAL) or OVA and then challenged with an aerosol of SAL or OVA. Twenty-four hours after the last aeroallergen challenge, the concentration of soluble ST2 in sera was measured by sandwich ELISA, and the expression of ST2L in splenocytes was detected by flow cytometry. The level of soluble ST2 was predominantly elevated in OVA-sensitized and -challenged (OVA/OVA) mice (Fig. 4*A*). In contrast, the production of soluble ST2 in other groups was low and showed no significant difference. However, soluble ST2 was below the detectable level in bronchoalveolar lavage fluids of any groups in our sandwich ELISA system (data not shown). Moreover, the expression of ST2L in splenocytes was apparently induced in OVA/OVA mice. On the other hand, the expression of ST2L in SAL/OVA mice was as low as that in untreated mice (Fig. 4*B* and data not shown). These results indicate that the expressions of soluble ST2 and ST2L were specifically induced in asthmatic mice by the combination of sensitization and challenge with OVA.

In addition, we also examined the protein expression of IL-33 in asthmatic mice. So far, a detection system such as ELISA for secreted murine IL-33 has not been developed. Therefore, we tried to detect IL-33 protein by Western blotting using commercially available anti-mouse IL-33 antibody. Cellular extracts were prepared from the thymus of asthmatic mice because the expression of IL-33 mRNA was highly induced in the thymus (Fig. 5*A*). However, we could detect neither the precursor nor the mature IL-33 protein in this experiment.

Expression of ST2, ST2L, and IL-33 mRNAs after the OVA Challenge—To investigate the expressions of the ST2 and IL-33 genes in various tissues of OVA/OVA mice, we performed a reverse transcription-PCR analysis (Fig. 5). Expression of the ST2 gene was induced in the thymus, lung, lymph node, spleen, and ovary after the last OVA challenge. However, the expression in the brain, heart, liver, kidney, and skeletal muscle was low or absent, as was the case for the testis (Fig. 5*A* and data not shown). Although the expression of the ST2 gene in the stomach was detected, the level of expression was not altered before and after the OVA challenge (data not shown). Interestingly, biphasic expression of the ST2 gene was observed in the thymus, lung, lymph node, and spleen. The expression of the ST2 gene was increased at 3 h, dropped at 6 h, and then increased again until 12 h or 24 h (Fig. 5). In addition, the expression profile was different in female and male mice. Expression of the ST2 gene was gradually induced in the ovary after the OVA challenge, but not in the testis. In the expression of the IL-33 gene, pronounced biphasic expression was observed in the thymus and lung (Fig. 5). IL-33 mRNA was expressed in the lymph node, ovary, and testis; however, the expression was hardly observed in the spleen. These results indicate that the expression of the ST2 gene is induced in immunological response-associated tissues after the OVA challenge and that the expression of the IL-33 gene is also induced in several tissues of asthmatic mice.

Suppression of the Production of Th2 Cytokines from IL-33-stimulated Splenocytes—A previous study showed that IL-33 induces the production of Th2 cytokines (9). To study the effects of soluble ST2 on the biological activity of IL-33, we analyzed the production of Th2 cytokines from splenocytes of asthmatic mice. We first examined whether rIL-33 binds to splenocytes using flow cytometry (Fig. 6*A*). Splenocytes were prepared from SAL/OVA and OVA/OVA mice at 24 h after the last OVA challenge. Recombinant IL-33 apparently bound to ST2L-positive splenocytes prepared from OVA/OVA mice. Next, we analyzed the production of Th1 and Th2 cytokines. Fig. 6*B* shows a scheme for the stimulation of splenocytes. The splenocytes were stimulated with OVA for activation of lymphocytes. The OVA-stimulated splenocytes were either untreated or treated with ST2-FLAG for 3 h. Subsequently, the splenocytes were left unstimulated or stimulated with rIL-33 for 48 h, followed by harvest of culture supernatants. Stimulation with rIL-33 specifically induced the productions of IL-4, IL-5, and IL-13 from splenocytes of OVA/OVA mice, whereas the production of these cytokines was reduced by pretreatment with ST2-FLAG (Fig. 6*C*). On the other hand, the production of IFN-γ was increased according to the reduction of Th2 cytokine production in splenocytes of OVA/OVA mice. Although the production of IFN-γ from splenocytes of SAL/OVA mice was also induced by the addition of IL-33 alone or ST2-FLAG plus IL-33, the reasons are presently unclear. Where the splenocytes of OVA/OVA mice were unstimulated with OVA, IL-33-induced production of Th2 cytokines was low (data not shown). These results suggest that IL-33 induces the production of Th2

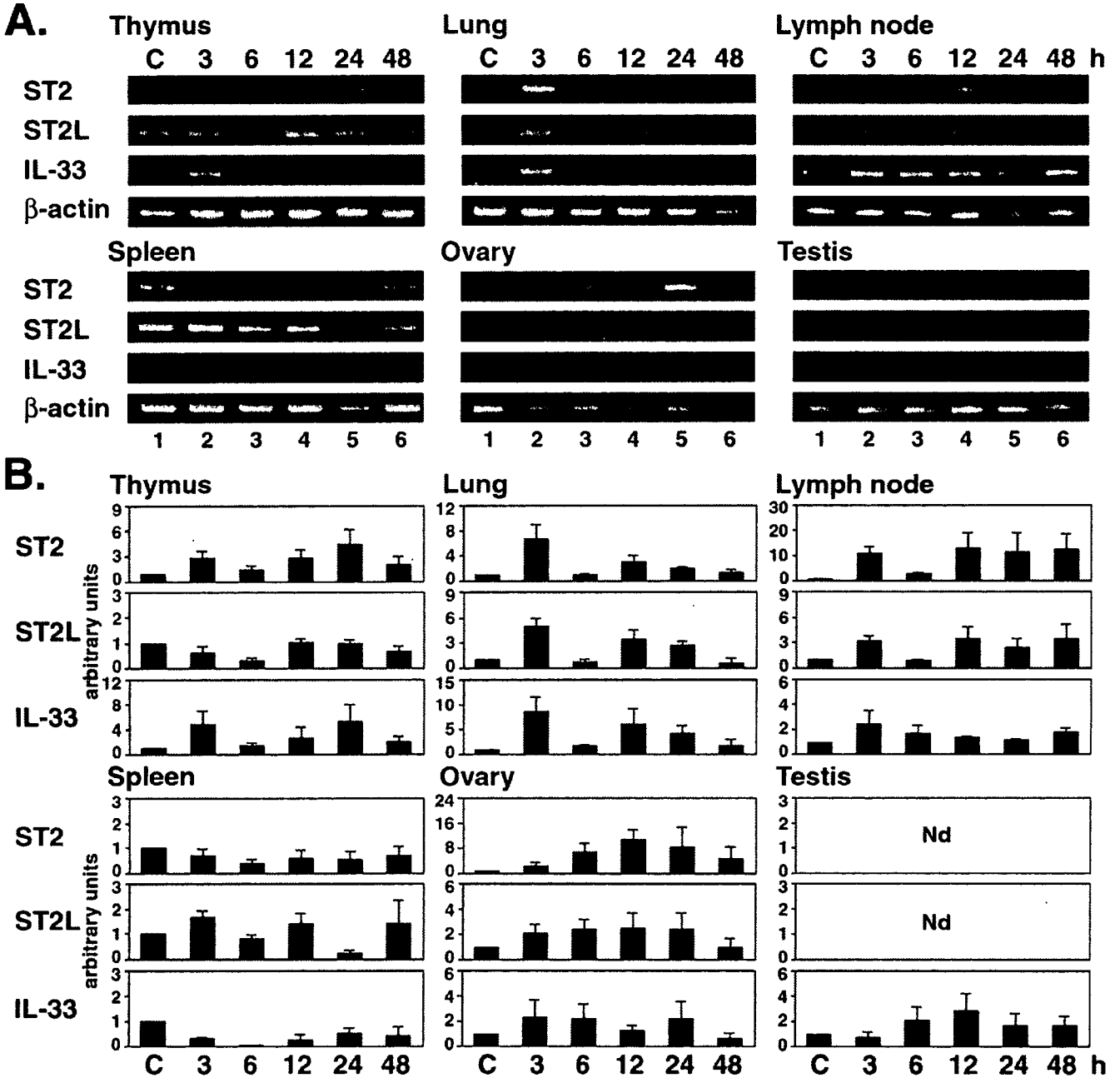

FIGURE 5. **Expression of ST2, ST2L, and IL-33 mRNAs after the last OVA challenge.** *A*, reverse transcription-PCR analysis of expression of ST2, ST2L, and IL-33 mRNAs in tissues of asthmatic mice. DNase I-treated total RNAs were prepared from tissues of untreated mice (*control; lanes C*) and OVA/OVA mice at the indicated time shown above each lane (*3–48 h*) after the last OVA challenge and then were subjected to reverse transcription-PCR analysis. β-Actin was detected as an internal control. PCR products were separated on 2% agarose gels. The data show one of three independent experiments. *B*, kinetic analysis of expression of ST2, ST2L, and IL-33 mRNAs. Densitometric analysis was performed using the public domain NIH Image program. Expression of ST2, ST2L, and IL-33 mRNAs was normalized with that of β-actin mRNA, and expression of control mice was given a reference value of 1. The data are shown as arbitrary units (means ± S.E.) from three independent experiments. *Nd*, no data for low level of gene expression.

cytokines from activated splenocytes via ST2L. Taken together, soluble ST2 suppresses the IL-33-induced production of Th2 cytokines.

DISCUSSION

This study has examined the regulation of IL-33 signaling by the soluble secreted form of the ST2 gene products (soluble ST2). We found that soluble ST2 has antagonistic effects on IL-33 signaling in allergic airway inflammation.

IL-33 is a member of the IL-1 cytokine family; the intracellular pathway of IL-33 signaling is similar to that of IL-1 signaling (9). We have studied IL-33 signaling using EL-4 cells stably expressing ST2L or IL-1RI (Figs. 1 and 3). IL-33 specifically bound to ST2L/EL-4 cells, but not to IL-1RI/EL-4 cells. The binding of IL-33 to ST2L induced the degradation of IκBα and subsequent activation of DNA binding activity of NF-κB. IL-33-induced DNA/NF-κB complex contained the p50 and p65 subunits. Furthermore, we found that soluble ST2 also bound to

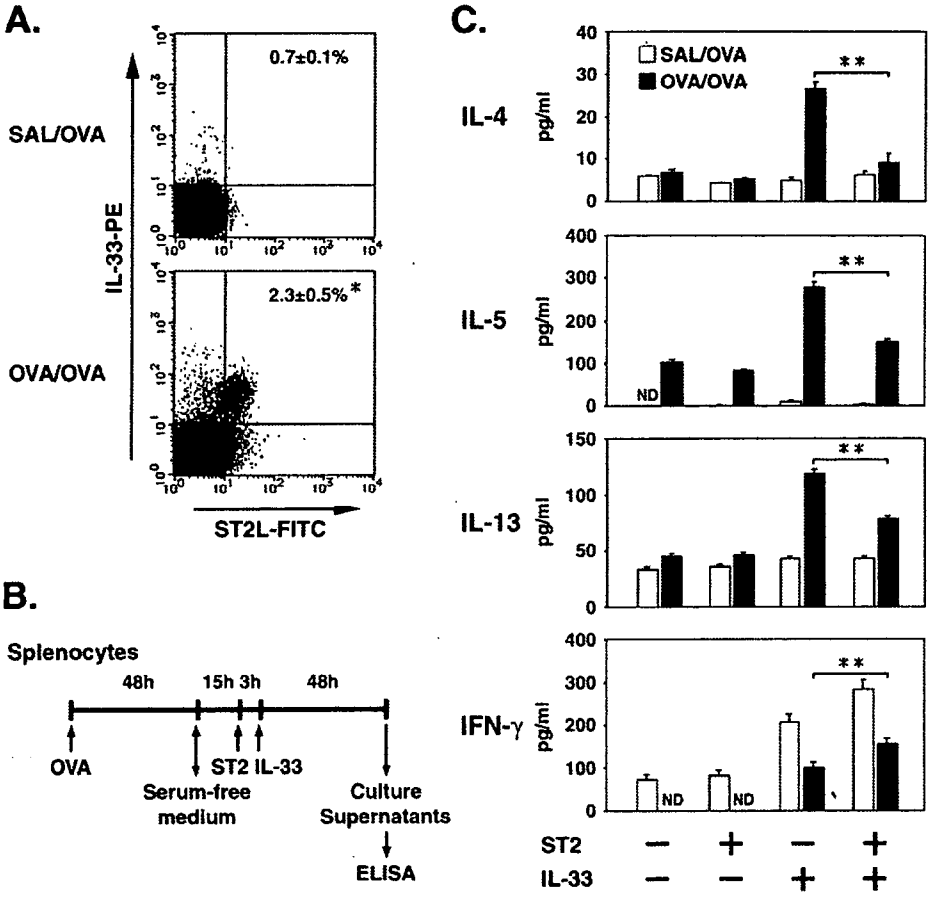

FIGURE 6. **Suppression of Th2 cytokine production from IL-33-stimulated splenocytes of asthmatic mice.** *A*, binding analysis of rIL-33 to splenocytes by flow cytometry. Splenocytes were prepared from SAL/OVA and OVA/OVA mice at 24 h after the last OVA challenge. The splenocytes (1×10^6 cells) were mixed with rIL-33 (1 μg) for 1 h. The splenocytes were stained with biotinylated anti-T7 tag antibody, RPE-conjugated streptavidin, and FITC-conjugated anti-mouse T1/ST2 antibody. Percentages of IL-33-bound ST2L-positive splenocytes are shown as the means ± S.E. ($n = 8$ mice in SAL/OVA, $n = 9$ mice in OVA/OVA; *, $p < 0.05$, OVA/OVA *versus* SAL/OVA). *B*, schematic diagram for stimulation of splenocytes. The splenocytes were prepared from SAL/OVA and OVA/OVA mice at 24 h after the last OVA challenge. Stimulation of splenocytes was performed as described under "Experimental Procedures." After the culture supernatants were harvested, the concentrations of IL-4, IL-5, IL-13, and IFN-γ were measured by ELISA. *C*, levels of Th1 and Th2 cytokines in culture supernatants. *White* and *black bars* indicate data obtained from splenocytes of SAL/OVA and OVA/OVA mice, respectively. The data are shown as the means ± S.E. ($n = 8$ mice in SAL/OVA, $n = 9$ mice in OVA/OVA; **, $p < 0.01$, IL-33 alone *versus* ST2 plus IL-33 in splenocytes of OVA/OVA mice). *ND*, not detected.

IL-33 and that pretreatment with soluble ST2 suppressed the IL-33-induced NF-κB activation in ST2L/EL-4 cells (Figs. 2 and 3). Thus, our results indicate that the binding activity of IL-33 for ST2L was inhibited by the formation of an ST2/IL-33 complex, leading to the suppression of IL-33 signaling.

Several studies have shown that soluble forms of cytokine receptors function as positive or negative regulators in the expression of cytokines and growth factors. The soluble form of IL-1 receptor type II (sIL-1RII), IL-4 receptor α-chain (sIL-4Rα), and IL-13 receptor α-chain 2 (sIL-13Rα2) have antagonistic effects on IL-1, IL-4, and IL-13 signalings, respectively (20–22). In contrast, the soluble IL-6 receptor α-chain (sIL-6Rα) has agonistic effects on IL-6 signaling and modulates the expression of chemokines (23, 24). Soluble forms of cytokine receptors are generated by several mechanisms including alternative splicing of pre-mRNA and proteolytic cleavage of receptors (25). In the case of the ST2 protein, soluble ST2 is generated by alternative splicing of pre-mRNA, and its amino acid sequence is mostly consistent with that of the extracellular domain of ST2L (1, 3). Therefore, it was a reasonable result that soluble ST2 possessed binding activity for IL-33. Besides soluble ST2 and ST2L, ST2V in humans and ST2LV in chickens have been reported as variant forms of the ST2 gene products (26–28). These variants might also be related to the regulation of IL-33 signaling because of containing the extracellular domain.

In patients and model mice of allergic asthma, the level of soluble ST2 was elevated in sera (14, 15), and the number of CD4-positive T cells expressing ST2L was increased in the lung and lymph nodes (29). On the other hand, the expression of IL-33 in allergic asthma is not investigated yet. In this study, we demonstrated that the expression of IL-33 mRNA was induced in several tissues after the OVA challenge in a murine model of asthma (Fig. 5). In addition, IL-33 bound to ST2L-positive splenocytes of asthmatic mice and induced the productions of IL-4, IL-5, and IL-13 (Fig. 6). Although we could not clarify a level and a time course for protein expression of IL-33, these results suggest that IL-33 expresses and functions as a cytokine in allergic asthma. Furthermore, we showed a detailed expression profile of the ST2 gene in asthmatic mice. The ST2 gene was predominantly expressed in the thymus, lung, lymph nodes, and spleen (Fig. 5). The expression of the ST2 gene in these tissues was regulated by the distal promoter (data not shown), which functions in Th2 cell-mediated immunological responses (16, 30). The biphasic expression pattern of ST2 mRNA corresponds to the production pattern of soluble ST2 in sera after the OVA challenge (15), suggesting that these tissues might be sources of soluble ST2. In addition, the level of soluble ST2 in sera was dramatically elevated in comparison with that of ST2L on the cell surfaces of splenocytes after the OVA challenge (Fig. 4). This drastic increase of the soluble ST2 concentration may contribute to the suppression of IL-33 signaling *in vivo*. In fact, pretreatment with soluble ST2 was effective for the suppression of IL-4, IL-5, and IL-13 productions from IL-33-stimulated splenocytes in asthmatic mice (Fig. 6). This negative effect on Th2 cytokine production was consistent with the results of therapeutic experiments using a recombinant soluble ST2-Fc protein or a soluble ST2 expression vector (7, 15). Thus, our results strongly support the paradigm that soluble ST2 neg-

atively regulates the production of Th2 cytokines in allergic airway inflammation.

Serum levels of soluble ST2 have been found to be elevated in various diseases such as rheumatoid arthritis, systemic lupus erythematosus, and idiopathic pulmonary fibrosis (31, 32), as well as asthma. In addition, soluble ST2 suppresses the production of inflammatory cytokines by stimulation with lipopolysaccharides in murine macrophages and THP-1 cells, derived from human monocytic leukemia (18, 33). Therefore, soluble ST2 may participate in the regulation of inflammatory cytokines besides Th2 cytokines.

NF-κB is a key regulator in the IL-33 signaling pathway, although it remains unclear how NF-κB regulates the expression of the Th2 cytokine genes. Previous studies using animal models have provided evidence that NF-κB plays an essential role in Th2 cell-mediated immunological responses. The p50-deficient ($p50^{-/-}$) and c-Rel-deficient ($c\text{-}Rel^{-/-}$) mice do not develop allergic airway inflammation (34, 35). Furthermore, p50 is required for the expression of transcription factor GATA-3, which regulates the expression of Th2 cytokine genes (36). Transgenic mice expressing dominant negative GATA-3 exhibit the inhibition of allergic inflammation (37). Hereafter, analysis of the downstream regulation of NF-κB is required to advance understanding of IL-33 signaling. In addition, the processing mechanism of the IL-33 protein has not been elucidated *in vivo*. A recent study reported that pre-IL-33 also functioned as a transcriptional repressor in nucleus besides acting as a cytokine (38). Therefore, the regulation for secretion of native IL-33 protein should be studied for better understanding of the biological and pathological functions of IL-33.

In conclusion, we showed the biological function of soluble ST2 *in vitro* and *in vivo*. We demonstrated that soluble ST2 suppresses the activation of NF-κB and the production of Th2 cytokines in IL-33 signaling, suggesting that this suppression leads to attenuation of allergic inflammatory responses in asthma. Furthermore, our findings may serve to advance knowledge in relation to the biological functions of IL-33 and therapeutic effects of soluble ST2 in allergic airway inflammation.

Acknowledgments—We thank Dr. K. Oshikawa and T. Ikahata for technical advice. We are also grateful to R. Izawa and H. Ohto-Ozaki for technical assistance.

REFERENCES

1. Tominaga, S. (1989) *FEBS Lett.* **258,** 301–304
2. Klemenz, R., Hoffmann, S., and Werenskiold, A. K. (1989) *Proc. Natl. Acad. Sci. U S. A.* **86,** 5708–5712
3. Yanagisawa, K., Takagi, T., Tsukamoto, T., Tetsuka, T., and Tominaga, S. (1993) *FEBS Lett.* **318,** 83–87
4. Gächter, T., Werenskiold, A. K., and Klemenz, R. (1996) *J. Biol. Chem.* **271,** 124–129
5. Yanagisawa, K., Naito, Y., Kuroiwa, K., Arai, T., Furukawa, Y., Tomizuka, H., Miura, Y., Kasahara, T., Tetsuka, T., and Tominaga, S. (1997) *J. Biochem. (Tokyo)* **121,** 95–103
6. Xu, D., Chan, W. L., Leung, B. P., Huang, F., Wheeler, R., Piedrafita, D., Robinson, J. H., and Liew, F. Y. (1998) *J. Exp. Med.* **187,** 787–794
7. Löhning, M., Stroehmann, A., Coyle, A. J., Grogan, J. L., Lin, S., Gutierrez-Ramos, J. C., Levinson, D., Radbruch, A., and Kamradt, T. (1998) *Proc. Natl. Acad. Sci. U. S. A.* **95,** 6930–6935
8. Lécart, S., Lecointe, N., Subramaniam, A., Alkan, S., Ni, D., Chen, R., Boulay, V., Pène, J., Kuroiwa, K., Tominaga, S., and Yssel, H. (2002) *Eur. J. Immunol.* **32,** 2979–2987
9. Schmitz, J., Owyang, A., Oldham, E., Song, Y., Murphy, E., McClanahan, T. K., Zurawski, G., Moshrefi, M., Qin, J., Li, X., Gorman, D. M., Bazan, J. F., and Kastelein, R. A. (2005) *Immunity* **23,** 479–490
10. Baekkevold, E. S., Roussigné, M., Yamanaka, T., Johansen, F. E., Jahnsen, F. L., Amalric, F., Brandtzaeg, P., Erard, M., Haraldsen, G., and Girard, J. P. (2003) *Am. J. Pathol.* **163,** 69–79
11. Dinarello, C. A. (1996) *Blood* **87,** 2095–2147
12. Tsutsui, H., Matsui, K., Okamura, H., and Nakanishi, K. (2000) *Immunol. Rev.* **174,** 192–209
13. Townsend, M. J., Fallon, P. G., Matthews, D. J., Jolin, H. E., and McKenzie, A. N. (2000) *J. Exp. Med.* **191,** 1069–1076
14. Oshikawa, K., Kuroiwa, K., Tago, K., Iwahana, H., Yanagisawa, K., Ohno, S., Tominaga, S., and Sugiyama, Y. (2001) *Am. J. Respir. Crit. Care Med.* **164,** 277–281
15. Oshikawa, K., Yanagisawa, K., Tominaga, S., and Sugiyama, Y. (2002) *Clin. Exp. Allergy* **32,** 1520–1526
16. Hayakawa, M., Yanagisawa, K., Aoki, S., Hayakawa, H., Takezako, N., and Tominaga, S. (2005) *Biochim. Biophys. Acta* **1728,** 53–64
17. Takagi, T., Yanagisawa, K., Tsukamoto, T., Tetsuka, T., Nagata, S., and Tominaga, S. (1993) *Biochim. Biophys. Acta* **1178,** 194–200
18. Takezako, N., Hayakawa, M., Hayakawa, H., Aoki, S., Yanagisawa, K., Endo, H., and Tominaga, S. (2006) *Biochem. Biophys. Res. Commun.* **341,** 425–432
19. Tago, K., Funakoshi, M., Mano, H., Yanagisawa, K., Hayakawa, M., Kuroiwa, K., Iwahana, H., Kasahara, T., and Tominaga, S. (2001) *Eur. J. Biochem.* **268,** 6526–6533
20. Giri, J. G., Wells, J., Dower, S. K., McCall, C. E., Guzman, R. N., Slack, J., Bird, T. A., Shanebeck, K., Grabstein, K. H., Sims, J. E., and Alderson, M. R. (1994) *J. Immunol.* **153,** 5802–5809
21. Sato, T. A., Widmer, M. B., Finkelman, F. D., Madani, H., Jacobs, C. A., Grabstein, K. H., and Maliszewski, C. R. (1993) *J. Immunol.* **150,** 2717–2723
22. Zhang, J. G., Hilton, D. J., Willson, T. A., McFarlane, C., Roberts, B. A., Moritz, R. L., Simpson, R. J., Alexander, W. S., Metcalf, D., and Nicola, N. A. (1997) *J. Biol. Chem.* **272,** 9474–9480
23. Peters, M., Jacobs, S., Ehlers, M., Vollmer, P., Müllberg, J., Wolf, E., Brem, G., Meyer zum Buschenfelde, K. H., and Rose-John, S. (1996) *J. Exp. Med.* **183,** 1399–1406
24. Hurst, S. M., Wilkinson, T. S., McLoughlin, R. M., Jones, S., Horiuchi, S., Yamamoto, N., Rose-John, S., Fuller, G. M., Topley, N., and Jones, S. A. (2001) *Immunity* **14,** 705–714
25. Levine, S. J. (2004) *J. Immunol.* **173,** 5343–5348
26. Tominaga, S., Kuroiwa, K., Tago, K., Iwahana, H., Yanagisawa, K., and Komatsu, N. (1999) *Biochem. Biophys. Res. Commun.* **264,** 14–18
27. Tago, K., Noda, T., Hayakawa, M., Iwahana, H., Yanagisawa, K., Yashiro, T., and Tominaga, S. (2001) *Biochem. Biophys. Res. Commun.* **285,** 1377–1383
28. Iwahana, H., Hayakawa, M., Kuroiwa, K., Tago, K., Yanagisawa, K., Noji, S., and Tominaga, S. (2004) *Biochim. Biophys. Acta* **1681,** 1–14
29. Gajewska, B. U., Swirski, F. K., Alvarez, D., Ritz, S. A., Goncharova, S., Cundall, M., Snider, D. P., Coyle, A. J., Gutierrez-Ramos, J. C., Stämpfli, M. R., and Jordana, M. (2001) *Am. J. Respir. Cell Mol. Biol.* **25,** 326–334
30. Shimizu, M., Matsuda, A., Yanagisawa, K., Hirota, T., Akahoshi, M., Inomata, N., Ebe, K., Tanaka, K., Sugiura, H., Nakashima, K., Tamari, M., Takahashi, N., Obara, K., Enomoto, T., Okayama, Y., Gao, P. S., Huang, S. K., Tominaga, S., Ikezawa, Z., and Shirakawa, T. (2005) *Hum. Mol. Genet.* **14,** 2919–2927
31. Kuroiwa, K., Arai, T., Okazaki, H., Minota, S., and Tominaga, S. (2001) *Biochem. Biophys. Res. Commun.* **284,** 1104–1108
32. Tajima, S., Oshikawa, K., Tominaga, S., and Sugiyama, Y. (2003) *Chest* **124,** 1206–1214
33. Sweet, M. J., Leung, B. P., Kang, D., Sogaard, M., Schulz, K., Trajkovic, V., Campbell, C. C., Xu, D., and Liew, F. Y. (2001) *J. Immunol.* **166,** 6633–6639

34. Yang, L., Cohn, L., Zhang, D. H., Homer, R., Ray, A., and Ray, P. (1998) *J. Exp. Med.* **188,** 1739–1750
35. Donovan, C. E., Mark, D. A., He, H. Z., Liou, H. C., Kobzik, L., Wang, Y., De Sanctis, G. T., Perkins, D. L., and Finn, P. W. (1999) *J. Immunol.* **163,** 6827–6833
36. Das, J., Chen, C. H., Yang, L., Cohn, L., Ray, P., and Ray, A. (2001) *Nat. Immunol.* **2,** 45–50
37. Zhang, D. H., Yang, L., Cohn, L., Parkyn, L., Homer, R., Ray, P., and Ray, A. (1999) *Immunity* **11,** 473–482
38. Carriere, V., Roussel, L., Ortega, N., Lacorre, D. A., Americh, L., Aguilar, L., Bouche, G., and Girard, J. P. (2007) *Proc. Natl. Acad. Sci. U. S. A.* **104,** 282–287

Prevention of diabetic retinopathy by intraocular soluble *flt-1* gene transfer in a spontaneously diabetic rat model

JUNICHI IDENO[1,2], HIROAKI MIZUKAMI[1], AKIHIRO KAKEHASHI[3], YUKA SAITO[3], TAKASHI OKADA[1], MASASHI URABE[1], AKIHIRO KUME[1], MASATOSHI KUROKI[4], MASANOBU KAWAKAMI[4], SHUN ISHIBASHI[2] and KEIYA OZAWA[1]

[1]Division of Genetic Therapeutics, Center for Molecular Medicine, [2]Department of Medicine, Division of Endocrinology and Metabolism, Jichi Medical University, Tochigi, Japan; [3]Department of Ophthalmology, [4]Department of Comprehensive Medicine I, Omiya Medical Center, Jichi Medical University, Saitama, Japan

Received August 11, 2006; Accepted October 2, 2006

Abstract. The number of patients suffering from diabetes mellitus is constantly rising worldwide, and diabetic retinopathy (DR) has become the most frequent cause of postnatal blindness. Vascular endothelial growth factor (VEGF) is known to play a central role during DR development. Thus, inhibiting the effects of VEGF may hamper the disease progression, and gene transfer of the soluble VEGF receptor *sflt-1* is an attractive approach for this purpose. However, the lack of suitable animal models hindered the evaluation of this strategy. Recently, the spontaneously diabetic non-obese Torii (SDT) rat was established and is considered as one of the ideal models for human DR. In this study, we evaluated the efficacy of gene therapy in SDT rats by using adeno-associated viral vectors (AAV-*sflt-1*) injected into the subretinal space. Thirty weeks later, the progression of DR was assessed by fluorescein angiography using three parameters; the presence of an avascular area, extensive hyperfluorescein and arterial narrowing. These changes were significantly less evident in the 'treated' eyes than in the control. No adverse effects were observed throughout the study. These results indicate that local *sflt-1* gene transfer inhibits DR progression in SDT rats and offers powerful therapeutic potential for the management of human DR.

Introduction

Diabetic retinopathy (DR) is one of the major complications of diabetes mellitus (DM), and the most frequent cause of postnatal blindness (1,2). The number of patients suffering from DM is steadily increasing worldwide (3), and the prevention of DR has become a matter of great importance. Unfortunately, the number of patients who are losing their vision due to DR is increasing despite the technological advancements, especially laser photocoagulation and vitreous surgery. Therefore, the development of a novel therapeutic approach to prevent DR progression has a vital significance.

Proliferative diabetic retinopathy (PDR) is an advanced form of DR characterized by neovascularization, vitreous hemorrhage and tractional retinal detachment. Although a number of biochemical changes, including increased polyol pathway activity (4,5), activation of protein kinase C (6-8) and accumulation of advanced glycation end-products (9,10) were reported in the development of PDR, vascular endothelial growth factor (VEGF), a potent endothelial cell-specific mitogen, plays a critical role in the angiogenesis of PDR (11-13). The actions of VEGF are mediated by the fms-like receptors, Flt-1 and Flk-1/KDR, which are expressed on vascular endothelial cells, and result in endothelial cell proliferation, migration, and increased vasopermeability with tyrosine kinase activity (14-17). Expression of VEGF is upregulated by hypoxia, and increased vitreous VEGF levels were observed in patients with PDR (12,18,19). Moreover, overexpression of VEGF by photo-receptors in transgenic mice promoted retinal neovascular-ization (20), whereas antagonists for VEGF suppressed neovascularization in the retina and iris (13,21,22). A soluble form of the VEGF receptor Flt-1 (sFlt-1) is the only known endogenous specific inhibitor for VEGF, and has drawn considerable attention for its potential clinical application in the inhibition of angiogenesis (23-28). It lacks the immuno-globulin-like domain, the transmembrane spanning region and the intracellular tyrosine-kinase domain. The anti-angiogenic activity of sFlt-1 results from the inhibition of VEGF by two mechanisms; the sequestration of VEGF and the formation of inactive heterodimers with membrane spanning isoforms of the VEGF receptors Flt-1 and KDR (26,29). Studies have shown that the administration of viral vectors encoding *sflt-1* inhibited retinal neovascularization in animal models (30,31). However, the actual merits of sFlt-1 in clinically relevant DR models have not been evaluated.

Correspondence to: Dr Hiroaki Mizukami, Division of Genetic Therapeutics, Center for Molecular Medicine, Jichi Medical University, 3311-1 Yakushiji, Shimotsuke, Tochigi 329-0498, Japan
E-mail: miz@jichi.ac.jp

Key words: diabetic retinopathy, gene therapy, *sflt-1*, spontaneously diabetic non-obese Torii rat, adeno-associated viral vector

Recently, a spontaneously diabetic, non-obese Torii (SDT) rat strain was established from the Sprague-Dawley lineage (32). The animals develop DM at ~20 weeks of age and later manifest DR, which is characterized by tractional retinal detachment, retinal hemorrhage, extensive venous dilatation, extensive hyperfluorescence and a non-perfusion area beyond 55 weeks of age (33). These findings are similar to those found in DR patients; therefore, the SDT rat is one of the best-suited models for studying human DR.

Adeno-associated viral (AAV) vectors are becoming popular in the field of gene therapy because of their safety and long-term effectiveness (34,35). A number of studies have demonstrated the efficacy of ocular gene therapy using AAV vectors (30,36), and vectors derived from serotype 5 (rAAV5) showed the highest utility for retinal gene transfer among serotypes tested (37-39). For this reason, we set out to test the utility of gene therapy on preventing DR in SDT rats using an rAAV5 vector encoding human *sflt-1* (rAAV5-*sflt-1*).

Materials and methods

rAAV vector construction and production. The *sflt-1* cDNA was amplified by PCR from the cDNA library of human umbilical vein endothelial cells (HUVEC). The *in vitro* effect of *sflt-1* expression was confirmed according to a method previously reported (40,41). Briefly, a plasmid was transfected into 293 cells with the Ca-phosphate method, the medium from 293 cells was added at specified dilutions to a 96-well plate containing HUVEC, and the cell density was assessed. An rAAV5 vector encoding *sflt-1* cDNA driven by the human cytomegalovirus (CMV) promoter (rAAV5-CMV-*sflt-1*) was constructed (Fig. 1). rAAV vectors were produced with an adenovirus-free system, and were purified by ultra-centrifugation through an Iodixanol (Axis-Shield PoC AS, Oslo, Norway) gradient followed by dialysis (42,43). The titers of the vector stocks were determined by quantitative dot-blot analysis using a BAS-1500 image analyzer (Fuji Film, Tokyo, Japan).

Animals. All animal experiments were performed in accordance with the standards in the Guide for the Care and Use of Laboratory Animals (NIH publication no. 85-23) and the institutional guidelines. Male SDT rats, provided by the Association for the Spontaneously Diabetic Torii Rat, were used in this study. Standard rodent diet and water were provided *ad libitum*. Casual blood glucose levels were measured by the glucose-oxydase method every four weeks using Glutest A (Sanwa Chemical, Tokyo, Japan). Glycosylated hemoglobin (HbA1c) was measured with a latex agglutination test (SRL, Tokyo, Japan), and plasma sFlt-1 levels were determined using a commercially available ELISA kit (Bender MedSystems, San Bruno, CA) at the end of the study.

Subretinal injection of vector solution. Rats at the age of 27 weeks were anesthetized with an intraperitoneal injection of pentobarbital sodium (1 mg/kg), and 0.4% oxybuprocaine chloride eye drops were used for additional analgesia. All surgical procedures were performed under a surgical microscope. The tip of a 10-mm 39-gauge nylon needle

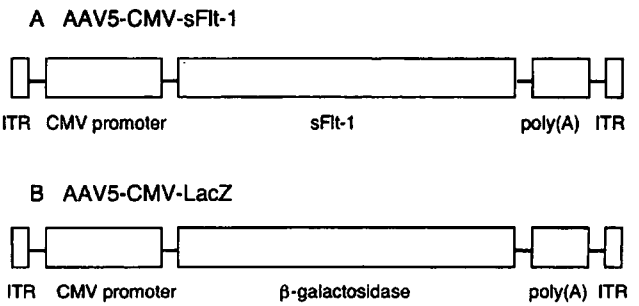

Figure 1. Structure of rAAV vectors. (A) rAAV5-CMV-*sflt-1* vector. (B) rAAV-CMV-*lacZ* vector. ITR, inverted terminal repeat of AAV serotype 5; CMV, human cytomegalovirus promoter; GH, human growth hormone first intron enhancer; Poly (A), SV40 early poly A.

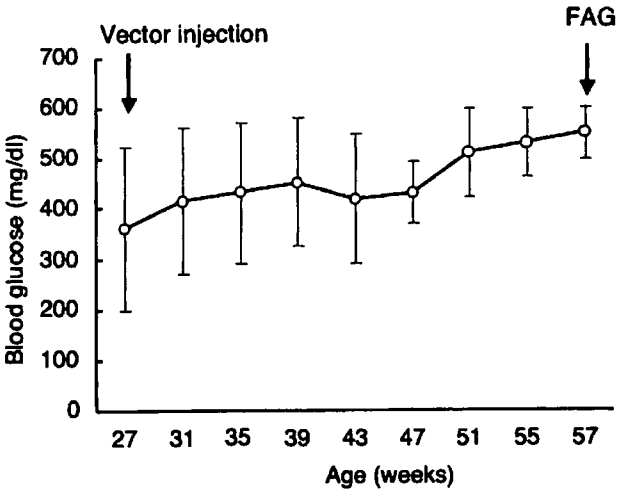

Figure 2. Blood glucose levels of animals during the study. All rats developed diabetes mellitus by the time of subretinal vector administration, and high glucose levels continued throughout the study. Data were shown as mean ± SD, (n=8). FAG, fluorescein angiography.

(Bausch & Lomb, Rochester, NY), mounted on a 10-μl Hamilton syringe, was inserted into the subretinal space through the sclera and ~10 μl of viral suspension was injected. Treated eyes received rAAV5-CMV-*sflt-1* ($4x10^{10}$ vector genome/eye) plus rAAV5 expressing ß-galactosidase (rAAV5-CMV-*lacZ*, $1x10^{10}$ vector genome/eye). Control eyes received only rAAV-CMV-*lacZ* ($1x10^{10}$ viral genome/eye).

Fluorescein-dextran microscopy and quantification of DR. Thirty weeks after the vector administration, the progression of DR was evaluated using fluorescein angiography (FAG). Cardiac perfusion was performed with 1 ml of PBS containing 50 mg of fluorescein-labeled dextran (fluorescein isothiocyanate-dextran; MW, $2x10^6$ daltons; Sigma, St Louis, MO), after administration of a lethal dose of pentobarbital sodium. The eyes were enucleated, the cornea and lens were removed, and the retina dissected from the eyecup. The retina was cut radially and flat-mounted on a glass slide without fixation. A drop of aqueous mounting medium (Crystal/mount, Biomeda